

Improved statistics for F-theory standard models

Martin Bies¹, Mirjam Cvetič^{2,3,4}, Ron Donagi^{3,2}, Marielle Ong³

¹*Department of Mathematics, RPTU Kaiserslautern-Landau,
Kaiserslautern, Germany*

²*Department of Physics and Astronomy, University of Pennsylvania,
Philadelphia, PA 19104-6396, USA*

³*Department of Mathematics, University of Pennsylvania,
Philadelphia, PA 19104-6396, USA*

⁴*Center for Applied Mathematics and Theoretical Physics, University of Maribor,
Maribor, Slovenia*

Much of the analysis of F-theory-based Standard Models boils down to computing cohomologies of line bundles on matter curves. By varying parameters one can degenerate such matter curves to singular ones, typically with many nodes, where the computation is combinatorial and straightforward. The question remains to relate the (a priori possibly smaller) value on the original curve to the singular one. In this work, we introduce some elementary techniques (pruning trees and removing interior edges) for simplifying the resulting nodal curves to a small collection of terminal ones that can be handled directly. When applied to the QSMs, these techniques yield optimal results in the sense that obtaining more precise answers would require currently unavailable information about the QSM geometries. This provides us with an opportunity to enhance the statistical bounds established in earlier research regarding the absence of vector-like exotics on the quark-doublet curve.

Contents

1. Introduction	3
2. Limit root bundles meet F-theory QSMs	7
3. Simplification techniques	11
3.1. Pruning leaves	11
3.2. Removing interior edges	14
3.2.1. Proofs of interior edge removal algorithm	17
3.3. Terminal graphs	19
3.3.1. Rational circuits	19
3.3.2. Elliptic circuits	22
4. Implications for F-theory QSMs	23
4.1. Improved statistics for “rational” QSMs	23
4.2. Improved statistics for “elliptic” QSMs	25
4.3. Absence of vector-like quark-doublets	28
5. Summary and outlook	29
A. Jumps on terminal graphs	33
A.1. Rational circuits	33
A.2. Elliptic circuits	40

1. Introduction

String Theory, a framework that seeks to unify quantum mechanics and general relativity, encompasses various regimes that offer valuable insights into the fundamental nature of the universe. Among these regimes, F-theory stands out as a non-perturbative approach that has garnered significant attention [1–3]. In this paper, we aim to enhance our comprehension of a prominent category of F-theory Standard Models known as F-theory QSMs [4], which represent the largest known class characterized by gauge coupling unification and the absence of chiral exotics. Our primary focus lies in the study of their vector-like spectra. Through this investigation, we make significant strides in refining our previous findings [5–7], which centered around the arithmetic aspects of Brill-Noether theory of root bundles on nodal curves.

F-theory is based on the powerful interplay between algebraic geometry and theoretical physics [1–3]. Here, singular elliptic fibrations play a pivotal role and significant progress has been made in studying these geometries over the years. An overview of the developing connections between F-theory and the Standard Model can be found in [8]. For a broader and relatively recent overview, see [9] and the references therein.

This research paper focuses on 4-dimensional compactifications of F-theory with $\mathcal{N} = 1$ supersymmetry for the purpose of phenomenological investigations. Our goal is to construct models of partial physics that closely align with the Standard Model of particle physics. We recall that 4-dimensional F-theory compactifications with $\mathcal{N} = 1$ supersymmetry exhibit chiral (super)fields in a specific representation \mathbf{R} of the gauge group, as well as their charge conjugate counterparts in the representation $\overline{\mathbf{R}}$. The difference in the number of the chiral fields in representations \mathbf{R} and $\overline{\mathbf{R}}$ is referred to as the chiral spectrum. Meanwhile, the separate numbers of fields in the representations \mathbf{R} and $\overline{\mathbf{R}}$ provide the vector-like spectrum. Since the Higgs is a vector-like pair, the study of vector-like pairs is inevitable in the quest for F-theory Minimal Supersymmetric Standard Models (MSSMs).

Significant efforts in perturbative String Theory have been dedicated to finding Standard model compactifications. This includes extensive work on the $E_8 \times E_8$ heterotic string [10–17] and intersecting branes models in type II String Theory [18–24] (also refer to [25] and references therein). While these perturbative String Theory compactifications realized the gauge sector of the Standard Model with its chiral spectrum, many constructions have shortcomings, such as the presence of exotic chiral or vector-like matter. The models that surpassed these obstacles and provided the first globally consistent construction of the MSSM in String Theory can be found in [13,14]. For further insight into the intricate global conditions relating to slope-stability of vector bundles, additional details are offered in [26,27].

The chiral fermionic spectrum of 4d $\mathcal{N} = 1$ F-theory compactifications is well understood. The physics is encoded in the geometry of an elliptically fibered Calabi-Yau space $\pi: Y_4 \rightarrow B_3$ and the chiral spectrum is fixed by the background gauge flux $G_4 = dC_3 \in H^{(2,2)}(Y_4)$ [28–36], where C_3 refers to the internal C_3 profile in the dual M-theory geometry. Consequently, many tools were developed to construct and count the primary vertical subspace of G_4 configurations and to work out the physical quantities determined by such fluxes [32,33,37–43]. Computationally, the most challenging condition is the G_4 -flux quantization condition $G_4 + \frac{1}{2}c_2(Y_4) \in H_{\mathbb{Z}}^4(Y_4)$. One often examines necessary conditions for a specific G_4 -flux to satisfy this quantization, and then proceeds with the resulting flux candidates under the assumption that the quantization condition is indeed satisfied. In applications of such toolkits, many globally consistent chiral F-theory models were presented [34,39,41,44,45]. This exploration culminated in the largest known group of explicit string vacua that realize the Standard Model gauge group with the exact chiral spectrum and gauge coupling unification. This class of F-theory models is known as the

Quadrillion F-theory Standard Models (QSMs) [4]. The G_4 -flux candidate in the F-theory QSMs satisfies “only” necessary conditions for flux quantization. We proceed under the assumption that the quantization condition is satisfied. This G_4 -flux candidate cancels the D3-tadpole and ensures that the $U(1)$ gauge boson remains massless.

The vector-like spectrum in F-theory depends not only on G_4 but also on C_3 . We refer to the F-theory “object” dual to C_3 as an F-theory gauge potential. Such gauge potentials can be thought of as elements of the Deligne cohomology of Y_4 (see [46] and references therein). Previous work, described in [46–48], utilizes the fact that certain subsets of the Deligne cohomology can be expressed in the Chow ring. This allowed us to compute line bundles $L_{\mathbf{R}}$ on the matter curves $C_{\mathbf{R}}$ in B_3 . These line bundles can be interpreted as the localization of gauge flux on matter curves $C_{\mathbf{R}}$ in the dual IIB picture, resulting in massive vector-like pairs on these curves. The massless zero modes on the matter curves are given by the sheaf cohomology groups of the line bundle $L_{\mathbf{R}}$, where $h^0(C_{\mathbf{R}}, L_{\mathbf{R}})$ represents the number of massless chiral superfields in the representation \mathbf{R} on $C_{\mathbf{R}}$, and $h^1(C_{\mathbf{R}}, L_{\mathbf{R}})$ represents the number of massless chiral superfields in the representation $\overline{\mathbf{R}}$ on $C_{\mathbf{R}}$.

By construction, the line bundles $L_{\mathbf{R}}$ are twists of one of the many spin bundles on $C_{\mathbf{R}}$. We recall that there are 2^{2g} inequivalent spin bundles on a smooth, irreducible genus g curve [49, 50]. Thus, one must investigate which spin bundles are compatible with the F-theory geometry, as well as their origin in the Deligne cohomology. To the best of the authors’ knowledge, such a study has not been conducted and the answer is unknown. In similar spirit, one usually approaches vector-like spectra by lifting an existing G_4 -flux to a gauge potential in the Deligne cohomology. Such lifts are not unique due to the intermediate Jacobian of Y_4 . It can also be hard to find a single lift in many situations. For instance, this happens in the QSMs [5], which is the origin of the root bundle program initiated in this work. Should we surpass these challenges, we still face a rather complicated interplay between the complex structure moduli of Y_4 and the line bundle cohomologies $h^i(C_{\mathbf{R}}, L_{\mathbf{R}})$. To illustrate this challenge, let us mention that even with advanced algorithms [51–54] and powerful supercomputers, the necessary computations could not be performed in realistic compactification geometries. So, the early works [46–48] focused on models with computationally simple geometries even though the compactifications exhibited unrealistically large numbers of chiral fermions.

Machine learning techniques have and are being employed in the string theory context. Such works include but are not limited to [55–59]. For a broader overview, the interested reader may wish to consult [60] and the references therein. In this spirit, in [61], machine learning techniques were employed to systematically investigate the complex structure dependence of line bundle cohomologies. A large dataset [62] of line bundle cohomologies for various complex structure moduli was generated using algorithms from [63]. By combining data science techniques and well-known results about Brill-Noether theory [64]¹, a quantitative exploration of the jumps in charged matter vector pairs in relation to the complex structure moduli of the matter curve $C_{\mathbf{R}}$ was conducted.

Inspite of the challenges we face, we find inspiration in the attractive aspects of F-theory QSMs [4] and the goal of providing explicit realizations of F-theory MSSMs. Therefore, our focus is on exploring the vector-like spectra within F-theory QSMs, specifically those localized on their five matter curves. This investigation was initiated in a previous study [5] and subsequently expanded upon in later works [6, 7]. This program was recently summarized in [67]. For yet more background information, the interested reader may consult [68].

¹For a contemporary presentation of Brill-Noether theory, the interested reader is referred to [65]. An earlier use of Brill-Noether theory in F-theory can be found in [66].

The first obstacle that we encounter is the lack of knowledge regarding the lift to the Deligne cohomology of the proposed G_4 -flux candidate in the F-theory QSMs. The second challenge involves allowing only for twists of spin bundles that align with this F-theory compactification. As we do not have answers to either of these questions, we have established a necessary condition that all induced line bundles $L_{\mathbf{R}}$ must satisfy. The initial study [5] revealed that on three of the five matter curves in the QSM geometry, the line bundle $L_{\mathbf{R}}$ must necessarily be a fractional power $P_{\mathbf{R}}$ of the canonical bundle on that particular matter curve $C_{\mathbf{R}}$. On the remaining two curves, the line bundles are, in addition, modified by contributions from Yukawa points. Such fractional power line bundles are known as root bundles, which are generalizations of spin bundles. Like spin bundles, root bundles are generally not unique. The mathematics suggests that different root bundles may arise from non-equivalent F-theory gauge potentials in Deligne cohomology; all of which produce the same G_4 -flux. However, not all root bundles that satisfy our constraints on $C_{\mathbf{R}}$ are necessarily induced by F-theory gauge potentials. In other words, just like the spin bundles, only specific root bundles on the matter curves are expected to be consistent with the F-theory geometry Y_4 . Therefore, an F-theory gauge potential gives rise to a set $\{P_{\mathbf{R}}\}$, which includes one root bundle for each matter curve $C_{\mathbf{R}}$. By repeating this process for all physically relevant F-theory gauge potentials, it is expected that only a subset of all root bundles on $C_{\mathbf{R}}$ will generally be obtained. Conversely, if we are given a set of root bundles $\{P_{\mathbf{R}}\}$ (one on each matter curve), then this set may not originate from an F-theory gauge potential. Namely, it is possible for one of the root bundles to not be induced at all or not be induced in combination with one of the other roots.

Determining which root bundles are physical, i.e. induced from an F-theory gauge potential, is crucial for gaining a comprehensive understanding of the physics involved. However, this task presents a significant challenge. Instead of directly addressing this question, the study conducted in [5] took a systematic approach by examining all root and all spin bundles on each matter curve. By adopting this method, it was possible to assign a specific root bundle to each matter curve (except for the Higgs curve) in a particular QSM geometry [4] such that their cohomologies exhibit the desired MSSM vector-like spectra. These bundles are obtained by deforming the smooth and irreducible physical matter curve $C_{\mathbf{R}}$ into a nodal curve $C_{\mathbf{R}}^{\bullet}$ and describing the root bundles on the latter using a diagrammatic representation called *limit roots* [69]. Counting the global sections of limit root bundles on the complete blow-up of $C_{\mathbf{R}}^{\bullet}$ can be accomplished using the techniques developed in [5].

In the expanded study conducted in [6], a computer algorithm was utilized to count all root bundles with three global sections on the complete blow-up of $C_{\mathbf{R}}^{\bullet}$ in 33 different families of QSM geometries. To accomplish this, families of toric spaces $B_3(\Delta^{\circ})$ associated with polytopes Δ° from the Kreuzer-Skarke list [70] were examined (see also [71] for a different study of these geometries in a string theory context). These toric spaces represent alternative desingularizations of toric K3-surfaces [72–76]. The study revealed that the structure of a canonical nodal curve $C_{\mathbf{R}}^{\bullet}$ and, consequently, the count of limit root bundles, solely depends on the polytope Δ° . These techniques were further refined in [7] to handle limit roots on “simple” partial blow-ups. The outcomes of the computer scan strongly indicate that the absence of vector-like exotics in the $(\mathbf{3}, \mathbf{2})_{1/6}$ representation is a highly probable scenario within the F-theory QSMs. It is essential to emphasize that this finding carries a statistical meaning, as the precise origin of the limit roots from F-theory gauge potentials has yet to be fully understood.

Results

This study builds upon previous works [5–7] and takes their techniques further. Previous research revealed that counting global sections of root bundles leads to exploring line bundle cohomology on nodal curves. Specifically, [6] focused on line bundle cohomology for disconnected nodal curves while [7] expanded the analysis to include tree-like nodal curves. In this study, we extend the investigation to line bundles on nodal curves with a non-zero first Betti number, i.e. circuits. To accomplish this, a two-step procedure is employed:

1. A line bundle on a difficult nodal curve is replaced by a line bundle on a simpler nodal curve, which we refer to as a *terminal circuit*.
2. It is demonstrated that there are only a finite number of terminal circuits for a fixed Betti number. Consequently, the terminal circuits are classified and line bundle cohomologies on this nodal curves are examined through a case-by-case analysis.

Based on the available data, we can confirm that our counts of global sections for root bundles are optimal. To achieve improved results, revisiting the QSM geometries and extracting more refined geometric information would be necessary. This includes acquiring information about the descent data of the root bundles and the precise line bundle divisor on elliptic components of the nodal curves. However, without this additional information, our computer scan [77] provides the best possible answer.

Having achieved the optimal outcome, we assess the probability of no vector-like exotics precisely on the quark-doublet curve. Across the union of all 33 distinct QSM families explored, this scenario is estimated to occur in at least 93.91% of all these configurations. This result strengthens the earlier findings that statistically support the likelihood of this desired physical scenario. However, it is crucial to note that these conclusions rely on the top-down origin of the root bundles, which we anticipate future research will clarify.

Estimating the likelihood of one exotic vector-like pair on the Higgs curve would be desirable, but is infeasible with our current computational techniques. However, we can use the compute Brill-Noether numbers on the quark-doublet curve to again at least some indications. Namely, our results show that this undesirable phenomenon of exactly one vector-like exotic on the quark-doublet curve occurs with probability of at most 5.17%. We view this result as a positive indication towards exactly one vector-like pair on the Higgs curve.

Outline

In section 2, we provide a concise overview of the previous findings. For a more comprehensive understanding, we direct interested readers to the original works [5–7]. This section also serves to justify the need for our more refined techniques, which expand upon the previous results. These advanced techniques are introduced in section 3. Of particular significance is the classification of the terminal graphs discussed in section 3.3. The investigation of jumps on these terminal graphs represents a technically challenging aspect of this research work. Further details and derivations can be found in appendix A.1 and appendix A.2. These techniques are then applied to the F-theory QSMs, and the implications are elaborated upon in section 4. Finally, we conclude this work with a summary and outlook in section 5.

2. Limit root bundles meet F-theory QSMs

We begin with a very brief revision on our root bundle program. The interested reader can find much more information in the original works [5–7] and the recent summary on this program in [67].

Vector-like spectra in F-theory are counted by the line bundle cohomologies of certain line bundles on the matter curves [46–48]. For the Quadrillion F-theory standard models [4], we could not determine the exact line bundle whose cohomologies count the vector-like spectra. However, it was possible to derive necessary and highly non-trivial constraints for these line bundles. Our initial study [5] showed that these line bundles $P_{\mathbf{R}}$ must be root bundles. To elaborate more on this finding, we first recall that the F-theory QSMs [4] are defined in terms of toric 3-folds with $\overline{K}_{B_3}^3 \in \{6, 10, 18, 30\}$. The five matter curves of these models are defined by sections $s_i \in H^0(B_3, \overline{K}_{B_3})$. In [5], we argued that the line bundles $P_{\mathbf{R}}$, whose cohomologies count the vector-like spectra, must necessarily satisfy the following conditions:

curve	root bundle constraint
$C_{(\mathbf{3},\mathbf{2})_{1/6}} = V(s_3, s_9)$	$P_{(\mathbf{3},\mathbf{2})_{1/6}}^{\otimes 2\overline{K}_{B_3}^3} = K_{(\mathbf{3},\mathbf{2})_{1/6}}^{\otimes (6+\overline{K}_{B_3}^3)}$
$C_{(\mathbf{1},\mathbf{2})_{-1/2}} = V(s_3, P_H)$	$P_{(\mathbf{1},\mathbf{2})_{-1/2}}^{\otimes 2\overline{K}_{B_3}^3} = K_{(\mathbf{1},\mathbf{2})_{-1/2}}^{\otimes (4+\overline{K}_{B_3}^3)} \otimes \mathcal{O}_{(\mathbf{1},\mathbf{2})_{-1/2}}(-30Y_1)$
$C_{(\overline{\mathbf{3}},\mathbf{1})_{-2/3}} = V(s_5, s_9)$	$P_{(\overline{\mathbf{3}},\mathbf{1})_{-2/3}}^{\otimes 2\overline{K}_{B_3}^3} = K_{(\overline{\mathbf{3}},\mathbf{1})_{-2/3}}^{\otimes (6+\overline{K}_{B_3}^3)}$
$C_{(\overline{\mathbf{3}},\mathbf{1})_{1/3}} = V(s_9, P_R)$	$P_{(\overline{\mathbf{3}},\mathbf{1})_{1/3}}^{\otimes 2\overline{K}_{B_3}^3} = K_{(\overline{\mathbf{3}},\mathbf{1})_{1/3}}^{\otimes (4+\overline{K}_{B_3}^3)} \otimes \mathcal{O}_{(\overline{\mathbf{3}},\mathbf{1})_{1/3}}(-30Y_3)$
$C_{(\mathbf{1},\mathbf{1})_1} = V(s_1, s_5)$	$P_{(\mathbf{1},\mathbf{1})_1}^{\otimes 2\overline{K}_{B_3}^3} = K_{(\mathbf{1},\mathbf{1})_1}^{\otimes (6+\overline{K}_{B_3}^3)}$

In this table, we make use of two polynomials: $P_H = s_2s_5^2 + s_1(s_1s_9 - s_5s_6)$ and $P_R = s_3s_5^2 + s_6(s_1s_6 - s_2s_5)$. It is important to note that the line bundles on both the Higgs curve $C_{(\mathbf{1},\mathbf{2})_{-1/2}}$ and the curve $C_{(\overline{\mathbf{3}},\mathbf{1})_{1/3}}$ are dependent on the Yukawa points $Y_1 = V(s_3, s_5, s_9)$ and $Y_3 = V(s_3, s_6, s_9)$, respectively. Furthermore, it is important to keep in mind that if two divisors D and E are linearly equivalent, i.e., $D \sim E$, then $n \cdot D \sim n \cdot E$ for any integer n . However, the converse is not true, and that is why we do not cancel common factors.

For instance, $P_{(\mathbf{3},\mathbf{2})_{1/6}}$ must be a $2\overline{K}_{B_3}^3$ -th root of the $(6 + \overline{K}_{B_3}^3)$ -th power of $K_{(\mathbf{3},\mathbf{2})_{1/6}}$. Hence, the name root bundles. It can be argued that solutions to the root bundle constraints in eq. (1) do exist, but are not unique. This is to be contrasted with the physics' expectation that only a subset of these roots is realized from F-theory gauge potentials in the Deligne cohomology $H_D^4(\widehat{Y}_4, \mathbb{Z}(2))$. Such top-down consideration were and still are beyond our reach. In addition, there are computational limitations that stop us from enumerating the huge number of root bundles on the Higgs curve and then working out their number of global sections. To circumvent both of these shortcomings, starting from our analysis in [6], we have therefore employed the following philosophy:

- Focus on F-theory QSM geometries, such that there are at least as many different F-theory gauge potentials as there are solutions to the root bundle constraint on the quark-doublet curve $C_{(\mathbf{3},\mathbf{2})_{1/6}}$. Then, at least statistically speaking, we could hope that every root bundle on the quark-doublet curve is realized from an F-theory gauge potential. It turned out that this condition is equivalent to $h^{2,1}(\widehat{Y}_4) \geq g$ where g is the genus of $C_{(\mathbf{3},\mathbf{2})_{1/6}}$ [6].

- Subsequently, we analyze the line bundle cohomologies of all root bundles on the quark-doublet systematically in order to draw conclusions about the presence/absence of vector-like exotics.

We thus make a selection among the F-theory QSMs. To this end, we recall that these geometries arise from desingularizations of toric K3-surfaces. Such desingularizations were first studied in [72] and correspond to 3-dimensional, reflexive lattice polytopes $\Delta \subset M_{\mathbf{R}}$ and their polar duals $\Delta^\circ \subset N_{\mathbf{R}}$ defined by $\langle \Delta, \Delta^\circ \rangle \geq -1$. The complete list of such 3-dimensional polytopes is available in [70]. Just as in [5–7] and denote the i -th polytope in this list as $\Delta_i^\circ \subset N_{\mathbf{R}}$. We denote the family of F-theory QSM geometries associated to the i -th 3-dimensional, reflexive lattice polytope Δ_i° in [70] by $B_3(\Delta_i^\circ)$. The different geometries in $B_3(\Delta_i^\circ)$ are one-to-one to the fine regular star triangulations of Δ_i° . Some quantities are the same for a family $B_3(\Delta_i^\circ)$, for instance \overline{K}_{B_3} , $h^{2,1}(\widehat{Y}_4)$ and the genus of $C_{(\mathbf{3},\mathbf{2})_{1/6}}$. It turns out that there are exactly 37 F-theory QSM families $B_3(\Delta_i^\circ)$ which satisfy $h^{2,1}(\widehat{Y}_4) \geq g$.

It thus remains to construct solutions for the root bundle constraint in eq. (1) on the matter curve $C_{(\mathbf{3},\mathbf{2})_{1/6}}^\bullet$ of these 37 QSM families and then to work out the line bundle cohomologies of those root bundles. Sadly, it turns out that this is a rather tough task for smooth, irreducible curves. Historic references indicating this obstacle include [49, 50]. Instead of working out the exact solutions, we have therefore opted for an approximation technique, which is based on the following two key insights:

- Root bundles on nodal curves are well understood and follow a diagrammatic pattern [69]. We refer the interested reader to [5] and [67] for more details.
- There is a canonical deformation $C_{(\mathbf{3},\mathbf{2})_{1/6}} \rightarrow C_{(\mathbf{3},\mathbf{2})_{1/6}}^\bullet$, such that the nodal curve $C_{(\mathbf{3},\mathbf{2})_{1/6}}^\bullet$ is the same for all spaces in $B_3(\Delta_i^\circ)$, i.e. depends only on the polytope Δ_i° . This was explained in large detail in [6].

It is worth noting that this is a rather impressive and stunning finding! Despite there being an enormous number of F-theory QSM geometries (around 10^{15}), it is possible to estimate the vector-like spectra of the majority of these setups from analyzing root bundles on only 37 different nodal curves!

Despite these pleasing features of nodal curves, we eventually want to go back and determine the cohomologies of root bundles on the initial smooth, irreducible matter curve $C_{(\mathbf{3},\mathbf{2})_{1/6}}$. Hence, we should study how cohomologies of root bundles $P_{\mathbf{R}}^\bullet$ on nodal curves relate to the cohomologies of root bundles $P_{\mathbf{R}}^\circ$ on the smooth irreducible curve. In principle, we can trace the roots $P_{\mathbf{R}}^\bullet$ along the deformation $C_{\mathbf{R}}^\bullet \rightarrow C_{\mathbf{R}}$ to find roots $P_{\mathbf{R}}$ on the original curve $C_{\mathbf{R}}$. While such a deformation can alter the number of global sections, it is known that it is known that the number of global sections is an upper semi-continuous function:

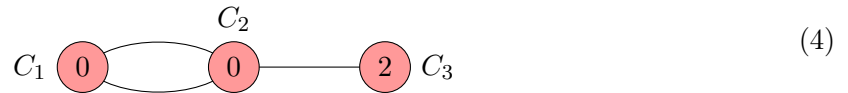
$$h^0(C_{\mathbf{R}}, P_{\mathbf{R}}) \leq h^0(C_{\mathbf{R}}^\bullet, P_{\mathbf{R}}^\bullet) = \chi(P_{\mathbf{R}}) + \delta, \quad \delta \in \mathbb{Z}_{\geq 0}. \quad (2)$$

In order to find roots for which the number of sections remains constant upon deformation to the original curve, we can look for instances where equality holds. One such instance is the generic case $\delta = 0$, in which $h^0(C_{\mathbf{R}}^\bullet, P_{\mathbf{R}}^\bullet) = \chi(P_{\mathbf{R}})$. This is because the number of sections is then already minimal on $C_{\mathbf{R}}^\bullet$ and therefore must remain constant throughout the deformation. As a result, the number of limit roots on the partial blow-ups $C_{\mathbf{R}}^\circ$ of the nodal curve $C_{\mathbf{R}}^\bullet$ that have the generic number of global sections provides a lower bound on the number of roots $P_{\mathbf{R}}$ without vector-like exotics. Indeed, this is exactly the situation that describes/approximates root bundles on $C_{(\mathbf{3},\mathbf{2})_{1/6}}$ without vector-like exotics.

In reassessing the 37 F-theory QSM families $B_3(\Delta_i^\circ)$ with $h^{2,1}(\widehat{Y}_4) \geq g$, we realized that for four of them, the canonical nodal quark-doublet curve $C_{(\mathbf{3},\mathbf{2})_{1/6}}^\bullet$ has a smooth, irreducible component whose genus is greater than one. This makes the global section counting for limit roots a lot harder, and so we decided to ignore those four QSM families. Consequently, we focused on the following 33 families of QSM geometries. Note that the numbers of fine regular star triangulations were worked out/estimated in [71].

Polytope	$\overline{K}_{B_3}^3$	N_{roots}	\check{N}_{FRST}	$\widehat{N}_{\text{FRST}}$
Δ_8°	6	12^8	3.867×10^{13}	2.828×10^{16}
Δ_4°	6	12^8	3.188×10^{11}	
Δ_{134}°	6	12^8	7.538×10^{10}	
$\Delta_{128}^\circ, \Delta_{130}^\circ, \Delta_{136}^\circ, \Delta_{236}^\circ$	6	12^8	3.217×10^{11}	
Δ_{88}°	10	20^{12}	5.231×10^{10}	1.246×10^{14}
Δ_{110}°	10	20^{12}	5.239×10^8	
$\Delta_{272}^\circ, \Delta_{274}^\circ$	10	20^{12}	3.212×10^{12}	2.481×10^{15}
Δ_{387}°	10	20^{12}	6.322×10^{10}	6.790×10^{12}
$\Delta_{798}^\circ, \Delta_{808}^\circ, \Delta_{810}^\circ, \Delta_{812}^\circ$	10	20^{12}	1.672×10^{10}	2.515×10^{13}
Δ_{254}°	10	20^{12}	1.568×10^{10}	
Δ_{52}°	10	20^{12}	1.248×10^8	
Δ_{302}°	10	20^{12}	5.750×10^7	
Δ_{786}°	10	20^{12}	9.810×10^8	
Δ_{762}°	10	20^{12}	1.087×10^{11}	2.854×10^{13}
Δ_{417}°	10	20^{12}	1.603×10^9	
Δ_{838}°	10	20^{12}	4.461×10^9	
Δ_{782}°	10	20^{12}	3.684×10^9	
$\Delta_{377}^\circ, \Delta_{499}^\circ, \Delta_{503}^\circ$	10	20^{12}	4.461×10^9	
Δ_{1348}°	10	20^{12}	4.285×10^9	
$\Delta_{882}^\circ, \Delta_{856}^\circ$	10	20^{12}	3.180×10^9	
Δ_{1340}°	10	20^{12}	4.496×10^9	
Δ_{1879}°	10	20^{12}	4.461×10^9	
Δ_{1384}°	10	20^{12}	7.040×10^9	

We conclude this section with an illustrative example of constructing limit roots and determining their number of global sections. This example is chosen to illustrate our key advances. The interested reader may consider this example as a motivation for the more involved study of these techniques in section 3. For this example, let us look at a nodal curve with three irreducible, smooth, rational components, whose dual graph Γ is as follows:



This means that the vertices represent the irreducible components and the edges correspond to the nodal singularities. On this curve, we consider a line bundle L with $\deg(L|_{C_i}) = (0, 0, 2)$, i.e. the degree of L restricted to the i -th component is exactly the number that we display in the above graph inside of the i -th vertex. It is worth recalling that this information does not

fix L uniquely. In order to uniquely specify L , we would have to specify the so-called descent data, which in this case, boils down to fixing one parameter $\lambda \in \mathbb{C}^*$ (see [78] for details). This parameter specifies that the sections on C_1 and C_2 agree up to λ at one of the two nodes in which they intersect, while the sections agree in all remaining nodes.

Let us now construct limit 2nd roots of this line bundle L . Note that $\beta_1(\Gamma) = 1$, so on a smooth, irreducible curve, there are $2^2 = 4$ roots. Here is how to construct the corresponding limit root. First, make a binary decision for each node. Namely, we decide whether to blow this node up or not. If we do, then this amounts to putting a bi-weight $1 - 1$ on the corresponding edge in the above graph and subtracting 1 from each of the adjacent vertices. Then, one removes the corresponding edge and tries to divide the resulting degrees by 2. If doing so leads to integer degrees on all vertices, we have encoded a limit root. In this case, this procedure leads to the following two admissible configurations:

$$\begin{array}{ccc}
 \begin{array}{c} C_1 \quad C_2 \quad C_3 \\ \textcircled{0} \text{---} \textcircled{0} \text{---} \textcircled{1} \\ \text{Limit root 1} \end{array} & & \begin{array}{c} C_1 \quad C_2 \quad C_3 \\ \textcircled{-1} \text{---} \textcircled{-1} \text{---} \textcircled{1} \\ \text{Limit root 2} \end{array}
 \end{array} \tag{5}$$

Limit root 1 is obtained by not blowing up any node, whereas limit root 2 is obtained by blowing up both nodes between C_1 and C_2 . Each of these graphs correspond according to the geometric multiplicity to $\mu = 2^{\beta_1(\Gamma)} = 2^1 = 2$ roots on a corresponding smooth, irreducible curve.

Now that we have enumerated the limit roots, it remains to compute the global sections. This is exactly where our new techniques appear. We begin by looking at limit root 1. Our simplification techniques for this line bundle on this nodal curve proceed as follows:

$$h^0 \left(\begin{array}{c} \textcircled{0} \text{---} \textcircled{0} \text{---} \textcircled{1} \end{array} \right) \stackrel{T1}{=} h^0 \left(\begin{array}{c} \textcircled{0} \text{---} \textcircled{0} \end{array} \right) + 1 \stackrel{T2}{=} h^0 \left(\begin{array}{c} \textcircled{0} \text{---} \textcircled{0} \end{array} \right) + 1. \tag{6}$$

The step $T1$ prunes a leaf while $T2$ removes an interior edge. We will give more details on these techniques in sections 3.1 and 3.2. By following these steps, we were able to reduce the original problem to a line bundle on an arguably simpler nodal curve:

$$\begin{array}{c} \textcircled{0} \text{---} \textcircled{0} \end{array} \tag{7}$$

This last graph cannot be simplified further, which is why we call such a configuration a *terminal graph*. We classify these terminal graphs in section 3.3 and analyze their number of global sections. In this case, it is not hard to see that there is exactly one global section provided that the descent data satisfies $\lambda = 1$. This corresponds to the canonical bundle on this nodal curve. In all other cases, we have no global sections. This is why we say that this terminal graph is jumping.

We now return to the second limit root. For this limit root, we obtain along the same lines:

$$h^0 \left(\begin{array}{c} \textcircled{-1} \quad \textcircled{-1} \text{---} \textcircled{1} \end{array} \right) \stackrel{T1}{=} h^0 \left(\begin{array}{c} \textcircled{-1} \quad \textcircled{-1} \end{array} \right) + 1. \tag{8}$$

For this limit root, there are always no global sections, irrespective of the descent data. We summarize this information as follows:

$$\begin{array}{c}
 \hline
 \begin{array}{cc}
 h^0 = 1 & h^0 \geq 1 \\
 \hline
 2 & 2 \\
 \hline
 \text{(Limit root 2)} & \text{(Limit root 1)} \\
 \hline
 \end{array}
 \end{array}
 \tag{9}$$

Certainly, the nodal curves encountered for the F-theory QSMs are more involved. But still, the steps to be taken are analogous to the above example. In the following section, we provide more details on the leaf pruning and removal of interior edges that eventually lead to the classification of terminal graphs in section 3.3. Subsequently, we return to the F-theory QSMs in section 4.

3. Simplification techniques

3.1. Pruning leaves

Let (C, L) be a pair consisting of a nodal curve C and line bundle L . Suppose that the dual graph Γ of C contains a tree (consisting of only rational components) that is attached to exactly one component (of genus 0 or 1) at exactly one node. We put forward an algorithm that prunes leaves repeatedly until the entire tree is removed.

Algorithm 1 (Algorithmic pruning of leaves). Suppose that Γ contains a leaf T , i.e. T is a vertex that is attached to exactly one vertex U of Γ at a nodal singularity p . If $d_T = \deg(L|_T) \geq 0$, then let $C' = C \setminus T$ and define a line bundle $L' = L|_{C'}$ on C' . Then,

$$h^0(C, L) = h^0(C', L') + d_T. \tag{10}$$

If $d_T < 0$, then let $C' = C \setminus T$ and define a new line bundle $L' = L \otimes_{\mathcal{O}_{C'}}(-p)$ on C' . In particular, it satisfies $L'|_U = L|_U \otimes \mathcal{O}_U(-p)$ and $L'|_{C' \setminus U} = L|_{C' \setminus U}$. Then,

$$h^0(C, L) = h^0(C', L'). \tag{11}$$

By repeating this procedure and pruning leaves repeatedly, we can remove subtrees of Γ . Let us explain the case where $d_T < 0$ further. If U has genus 0, then replacing L with L' amounts to replacing d_U with $d_U - 1$. This is because line bundles on rational curves are uniquely specified by their degree. However, this is no longer true when U has genus 1. That is, non-isomorphic bundles on an elliptic curve can have the same degree and this adds ambiguity when calculating h^0 . Indeed, the Riemann-Roch Theorem states that for a degree d line bundle L on an elliptic curve E ,

$$h^0(E, L) = \begin{cases} d, & \text{if } d \geq 1, \\ 0 \text{ or } 1, & \text{if } d = 0, \\ 0, & \text{if } d < 0. \end{cases}
 \tag{12}$$

So if the pruning leads to a degree 0 line bundle on the elliptic component, then we can only find a lower bound for h^0 . For example, let $d < 0$ and consider the curve C and line bundle L :



The degree 1 line bundle on E is either $\mathcal{O}_E(p)$, where p is the node on E , or $\mathcal{O}_E(q)$ for some other point $q \in E$. Applying the algorithm involves pruning C_1 and demanding that sections of the line bundle on E have a zero at p . This leads to the weighted dual graph Γ' :

$$\begin{array}{c} \textcircled{0} \\ E \end{array} \quad (14)$$

At this stage, the line bundle on E is either $\mathcal{O}_E(p - p) = \mathcal{O}_E$, which has $h^0 = 1$, or $\mathcal{O}_E(q - p)$, which has $h^0 = 0$.

We illustrate this algorithm with a few examples. Here, genus 0 components are marked in pink while genus 1 components are marked in green. When it is possible for two vertices to be connected to each other by more than one edge, we draw two dashed edges between the two vertices.

Example 3.1 (When the tree is based at a rational component). Let (C, L) be depicted by the following graph Γ . Suppose that Γ contains a tree, consisting of rational components C_1 to C_4 , that is connected to a rational component R . Let S be the complement of the tree in Γ .

The diagram shows a sequence of components: $S \setminus R$ (a small orange circle with d), R (a pink circle with $d_R = -2$), C_1 (a pink circle with $d_1 = 0$), C_2 (a pink circle with $d_2 = 3$), C_3 (a pink circle with $d_3 = -2$), and C_4 (a pink circle with $d_4 = 1$). Dashed edges connect $S \setminus R$ to R . Solid edges connect R to C_1 , C_1 to C_2 , C_2 to C_3 , and C_3 to C_4 .

First, prune the leaf C_4 from C_3 . This leads to the following pair (C', L') :

The diagram shows the components after pruning C_4 : $S \setminus R$ (orange circle with d), R (pink circle with $d_R = -2$), C_1 (pink circle with $d_1 = 0$), C_2 (pink circle with $d_2 = 3$), and C_3 (pink circle with $d_3 = -2$). Dashed edges connect $S \setminus R$ to R . Solid edges connect R to C_1 , C_1 to C_2 , and C_2 to C_3 .

Since $d_4 \geq 0$, we have that $h^0(C, L) = h^0(C', L') + 1$. Next, prune C_3 from C_2 . This leads to the following pair (C'', L'')

The diagram shows the components after pruning C_3 : $S \setminus R$ (orange circle with d), R (pink circle with $d_R = -2$), C_1 (pink circle with $d_1 = 0$), and C_2 (pink circle with $d_2 = 2$). Dashed edges connect $S \setminus R$ to R . Solid edges connect R to C_1 and C_1 to C_2 .

Note that d_2 was reduced by 1 since $d_3 = -2 < 0$. We have that $h^0(C, L) = h^0(C'', L'') + 1$. Next, prune C_2 from C_1 , which leads to the following pair (C''', L''') :

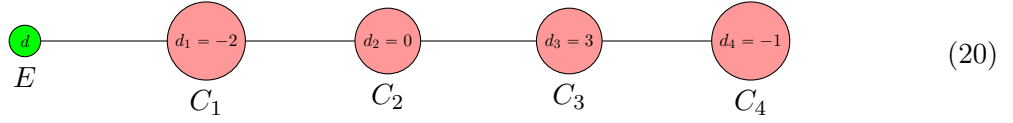
The diagram shows the components after pruning C_2 : $S \setminus R$ (orange circle with d), R (pink circle with $d_R = -2$), and C_1 (pink circle with $d_1 = 0$). Dashed edges connect $S \setminus R$ to R . A solid edge connects R to C_1 .

Since $d_2 = 2$, the algorithm tells us to increase the offset by 2. Thus, $h^0(C, L) = h^0(C''', L''') + 3$. Next, prune C_1 from R and obtain the pair $(C'''' = S, L''')$.

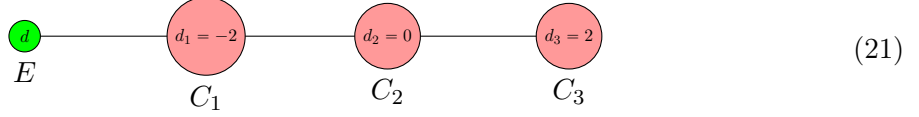
The diagram shows the final components after pruning C_1 : $S \setminus R$ (orange circle with d) and R (pink circle with $d_R = -2$). Dashed edges connect $S \setminus R$ to R .

Since $d_1 = 0$, the offset is 0 and $h^0(C, L) = h^0(C''', L''') + 3$.

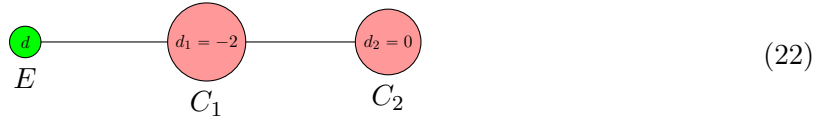
Example 3.2 (When the tree is based at an elliptic component). Suppose that Γ contains a tree, consisting of rational components C_1 to C_4 , that is connected to an elliptic component E .



First, prune C_4 from C_3 . Since $d_4 < 0$, we replace d_3 with $d_3 - 1$. This leads to the pair (C', L') :



We have that $h^0(C, L) = h^0(C', L')$. Next, prune C_3 from C_2 . This leads to the pair (C'', L'') :



We have that $h^0(C, L) = h^0(C'', L'') + 2$. Pruning C_2 from C_1 leads to the pair (C''', L''') :



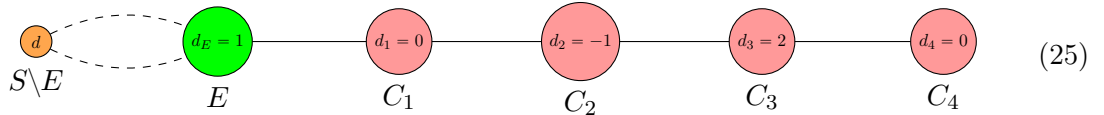
We have that $h^0(C, L) = h^0(C''', L''') + 2$. Next, prune the leaf C_1 from E . Since $d_1 < 0$, we replace d with $d - 1$. This leaves us with the pair $(C'''' = E, L''')$:



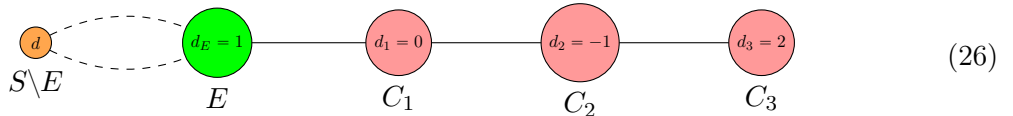
The final formula for $h^0(C''', L''')$ is

$$h^0(C''', L''') = h^0(E, L''') + 2 = 2 + \begin{cases} d, & \text{if } d \geq 2, \\ 0 \text{ or } 1, & \text{if } d = 1, \\ 0, & \text{if } d < 1. \end{cases}$$

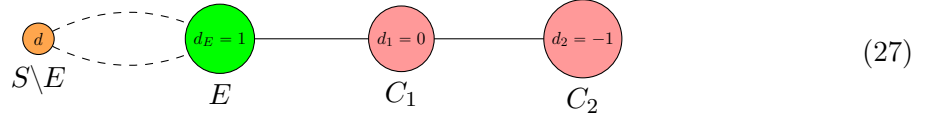
Example 3.3 (When the tree is based at a elliptic component). Let (C, L) be depicted by the following graph Γ . Suppose that Γ contains a tree, consisting of rational components C_1 to C_4 , that is connected to an elliptic component E . Let S be the complement of the tree in Γ .



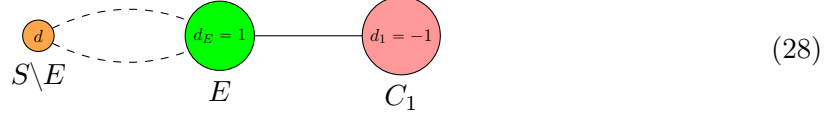
First, prune the leaf C_4 from C_3 . This leads to the following pair (C', L') :



We have that $h^0(C, L) = h^0(C', L')$. Next, prune C_3 from C_2 . This leads to the pair (C'', L'') :



Since $d_3 \geq 0$, we have that $h^0(C, L) = h^0(C'', L'') + 2$. Next, prune C_2 from C_1 , which leads to the following pair (C''', L''') :



Since $d_2 < 0$, we reduce d_1 by 1 and we have $h^0(C, L) = h^0(C''', L''') + 2$. Next, prune C_1 from E and obtain the pair $(C'''' = S, L''')$.



Since $d_1 < 0$, we reduce d_E by 1 and we have $h^0(C, L) = h^0(C''''', L''''') + 2$.

3.2. Removing interior edges

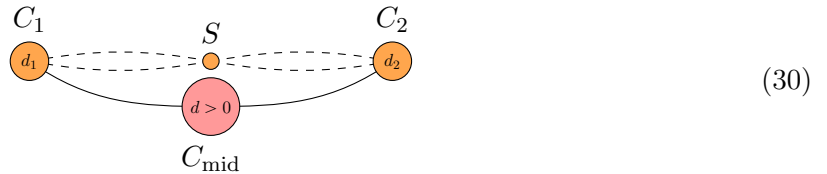
We present our second major technique that simplifies the pair (C, L) . Suppose that a rational component C_{mid} of C is connected to two other components C_1 and C_2 (not necessarily distinct) via a single edge each. We call C_{mid} and the two half-edges emanating from it an *interior edge*.

Algorithm 2. Suppose that C contains an interior edge C_{mid} that meets C_1 at node p_1 and C_2 at node p_2 . Let $d = \deg(L|_{C_{\text{mid}}})$.

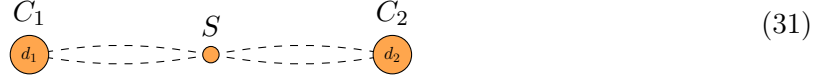
1. If $d > 0$, let $C' = C \setminus C_{\text{mid}}$ and $L' = L|_{C'}$. Then, $h^0(C, L) = h^0(C', L') + d - 1$.
2. If $d < 0$, let $C' = C \setminus C_{\text{mid}}$ and define a new line bundle $L' = L \otimes \mathcal{O}_{C'}(-p_1 - p_2)$ on C' . Then, $h^0(C, L) = h^0(C', L')$.
3. If $d = 0$, form a new curve C' by removing C_{mid} from C and joining the remaining half-edges to form an edge. This gives rise to a map $\pi : C \rightarrow C'$ that collapses the interior edge to the new node. Define the sheaf $L' = \pi_*(L)$ on C' , which is a line bundle because $d = 0$. Then, $h^0(C, L) = h^0(C', L')$.

Again, if C_i is rational, then twisting L_{C_i} by $\mathcal{O}_{C_i}(-p_i)$ in the algorithm amounts to decreasing $\deg(L|_{C_i})$ by 1. We illustrate the different cases of the algorithm in the following figures. We mark the vertex orange if its genus is either 0 or 1.

Figure 3.4 (Case 1: $d > 0$). Consider the pair (C, L) given by the following graph and let $S = C \setminus (C_1 \cup C_{\text{mid}} \cup C_2)$. Denoting $d_i = \deg(L|_{C_i})$, we have that

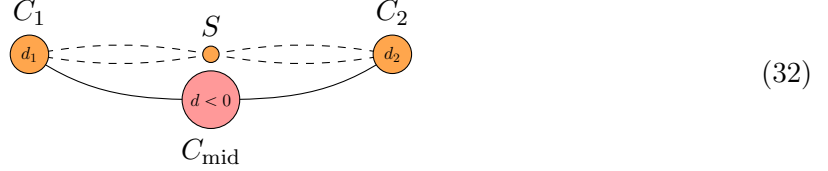


By the algorithm, we define a new pair $(C' = C \setminus C_{\text{mid}}, L' = L|_{C'})$, which is given by the following graph:

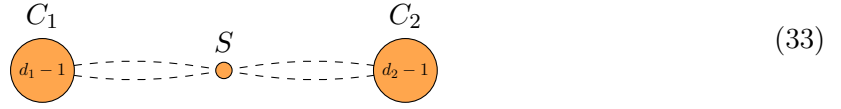


We have that $h^0(C, L) = h^0(C', L') + d - 1$.

Figure 3.5 (Case 2: $d < 0$). Consider the pair (C, L) given by the following graph and let $S = C \setminus (C_1 \cup C_{\text{mid}} \cup C_2)$. Denoting $d_i = \deg(L|_{C_i})$, we have that

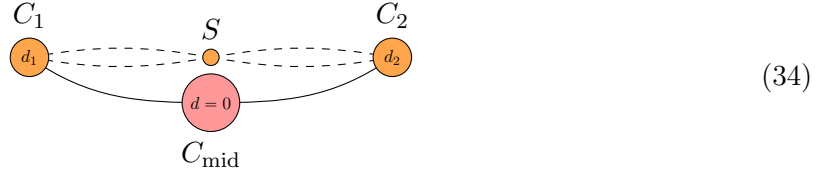


By the above algorithm, we define a new pair (C', L') by the following graph:

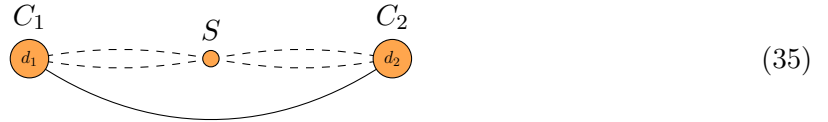


Then, $h^0(C, L) = h^0(C', L')$.

Figure 3.6 (Case 3: $d = 0$). Consider the pair (C, L) given by the following graph and let $S = C \setminus (C_1 \cup C_{\text{mid}} \cup C_2)$. Denoting $d_i = \deg(L|_{C_i})$, we have that



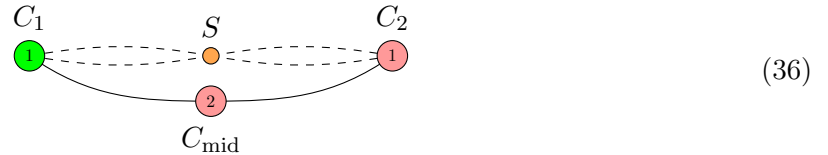
By the algorithm, define a new pair (C', L') given by the following graph:



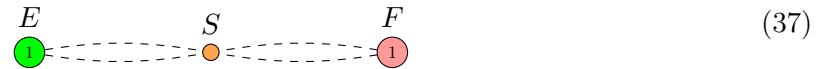
Then, $h^0(C, L) = h^0(C', L')$,

We will now apply the algorithm to a few examples.

Example 3.7. Consider the pair (C, L) given by the following graph:

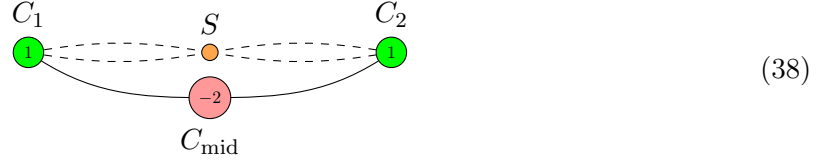


Since $\deg(L|_{C_{\text{mid}}}) > 0$, the algorithm tells us to form the new pair (C', L') given by the graph:

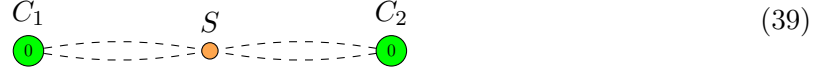


Then, $h^0(C, L) = h^0(C', L') + 2 - 1 = h^0(C', L') + 1$.

Example 3.8. Consider the pair (C, L) given by the following graph:

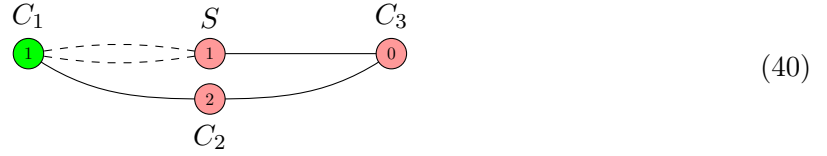


Since $\deg(C_{\text{mid}}) < 0$, the algorithm tells us to remove C_{mid} , adjust the degrees and form the new pair (C', L') :

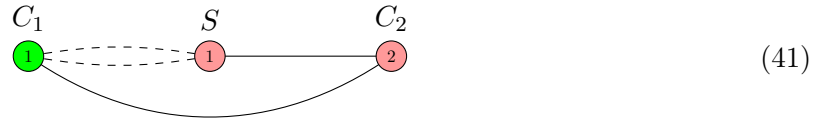


Then, $h^0(C, L) = h^0(C', L')$. Since there are degree 0 bundles on C_1 and C_2 , we can only compute the lower bound of h^0 .

Example 3.9. Consider the pair (C, L) given by the following graph:



We can first remove C_3 using the algorithm. Since $\deg(L|_{C_3}) = 0$, we remove C_2 and join the half-edges to produce a new pair (C', L') :

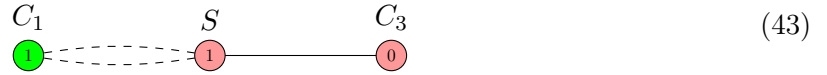


Then, $h^0(C, L) = h^0(C', L')$. To remove C_2 , we apply the algorithm to form a new pair (C'', L'') :



Then, $h^0(C, L) = h^0(C'', L'') + 1$.

Alternatively, we could remove C_2 first. This involves forming a new curve (\tilde{C}', \tilde{L}') :



Then, $h^0(C, L) = h^0(\tilde{C}', \tilde{L}') + 1$. Next, we view C_3 as a leaf and prune it by forming the new pair $(\tilde{C}'', \tilde{L}'')$:



Then, $h^0(C, L) = h^0(\tilde{C}'', \tilde{L}'') + 1$. Note that $(\tilde{C}'', \tilde{L}'') = (C'', L'')$. So, both procedures conclude with the same result.

We can also apply this to remove interior edges connected to the same curve component.

Example 3.10 (When $C_1 = C_2$). Consider the pair (C, L) given by the following graph:



If $d = 0$, the algorithm tells us to remove C_{mid} and join the half-edges to form the new pair (C', L') :



Then $h^0(C, L) = h^0(C', L')$. If $d < 0$, the algorithm tells us to remove C_{mid} and adjust the degrees on C_1 in the following way to obtain the new pair (C', L') :



By Riemann-Roch we have that:

$$h^0(C, L) = h^0(C', L') = \begin{cases} d_1 - 2, & \text{if } d_1 > 2, \\ 0 \text{ or } 1, & \text{if } d_1 = 2, \\ 0, & \text{if } d_1 < 2. \end{cases} \quad (48)$$

To explain the $d_1 = 2$ case further, let p and q be the nodes on C_1 . Applying the algorithm involves demanding that the line bundle sections on C_1 vanish at p and q . If $L|_{C_1} \cong \mathcal{O}_{C_1}(p+q)$, then the algorithm results in the line bundle $L' = \mathcal{O}_{C_1}(p+q-p-q) = \mathcal{O}_{C_1}$, which has $h^0(C', L') = 1$. Otherwise, it is a non-trivial, degree 0 line bundle on C_1 and $h^0(C', L') = 0$.

If $d > 0$, we remove C_{mid} and obtain the new pair (C', L') . The algorithm states that $h^0(C, L) = h^0(C', L') + d - 1$.



3.2.1. Proofs of interior edge removal algorithm

In this section, we present a case-by-case proof of the interior-edge-removal techniques presented earlier. Some of these results could be proved more efficiently using techniques from algebraic geometry but we choose to leave the elementary proofs for accessibility. Suppose that a pair (C, L) contains an interior edge C_{mid} between two components C_1 and C_2 . Denote $d = \deg(L|_{C_{\text{mid}}})$ and $d_i = \deg(L|_{C_i})$. Since PGL_2 acts on \mathbb{P}^1 transitively, we may assume that C_{mid} meets C_1 and C_2 at the points $[1 : 0]$ and $[0 : 1]$ on C_{mid} respectively.

Case 1: $d > 0$.

Lemma 1. If $C' = C \setminus C_{\text{mid}}$ and $L' = L|_{C'}$, then $h^0(C, L) = h^0(C', L') + d - 1$.

Proof

Let n_1, n_2 be the nodes at which C_{mid} is attached to C_1 and C_2 . Observe that we have the following:

$$h^0(C, L) = h^0(C' \cup C_{\text{mid}}, L) \quad (50)$$

$$\geq h^0(C', L') + h^0(C_{\text{mid}}, L|_{C_{\text{mid}}}) - h^0(\{n_\alpha, n_\beta\}, L|_{\{n_\alpha, n_\beta\}}) \quad (51)$$

$$= h^0(C', L') + d - 1. \quad (52)$$

To prove that equality is achieved, we need to show that the nodes impose exactly two independent conditions. Let $[z : w]$ be the coordinates on $C_{\text{mid}} \cong \mathbb{P}^1$. Then, any section $s \in H^0(C_{\text{mid}}, L)$ is of the form

$$s([z : w]) = \sum_{i=0}^d \gamma_i z^i w^{d-i}, \quad \gamma_i \in \mathbb{C}. \quad (53)$$

Let $s_1 \in H^0(C_1, L|_{C_1})$ and $s_2 \in H^0(C_2, L|_{C_2})$ be arbitrary sections. Then, s coincides with s_1 at the node $[1 : 0]$ and s coincides with s_2 at the node $[0 : 1]$ up to descent data, i.e.

$$\gamma_0 = s([1 : 0]) = \lambda_1 s_1([1 : 0]), \quad \gamma_d = r = s([0 : 1]) = \lambda_2 s_2([0 : 1]), \quad (54)$$

where $\lambda_1, \lambda_2 \in \mathbb{C}^*$ are descent data parameters assigned at the nodes. These equations are well-defined in the sense that scaling the intersection points on \mathbb{P}^1 does not change $h^0(C, L)$. Indeed, the basis sections of $H^0(C, L)$ will differ by a $\text{PGL}_2(\mathbb{C})$ -transformation under such scaling. Hence, these equations are two independent conditions imposed onto $H^0(C_{\text{mid}}, L|_{C_{\text{mid}}})$. So, the result follows. \blacksquare

Case 2: $d < 0$.

Lemma 2. Let (C', L') be the pair defined as in Algorithm 2. Then, $h^0(C, L) = h^0(C', L')$.

Proof

Suppose $d_i = \deg(L|_{C_i}) > 0$ and p_i be the nodes on C_i for $i = 1, 2$. Then, sections $s_1 \in H^0(C_1, L|_{C_1})$ and $s_2 \in H^0(C_2, L|_{C_2})$ satisfy the following gluing conditions at the nodes regardless of the descent data:

$$s_1(p_1) = 0, \quad s_2(p_2) = 0. \quad (55)$$

Demanding s_i to vanish at p_i amounts to twisting the line bundle on C_i by $O_{C_i}(-p_i)$. Hence, the result $h^0(C, L) = h^0(C', L')$ follows for $d_i > 0$.

If one of the d_i is negative, then the zero section on the corresponding component C_i glues to the zero section on C_{mid} uniquely. Since $d_i < 0$, twisting the line bundle on C_i still results in a negative degree $d_i - 1 < 0$. Hence, $h^0(C_i, L'|_{C_i}) = h^0(C_i, L|_{C_i}) = 0$ and the result follows. \blacksquare

Case 3: $d = 0$.

Lemma 3. Suppose that C_{mid} met C_1 at the node $p_1 \in C_1$ and C_2 at the node $p_2 \in C_2$. Remove C_{mid} and join the half-edges together so that C_1 meets C_2 at $p_1 \in C_1$ and $p_2 \in C_2$. This gives rise to a map $\pi : C \rightarrow C'$ that collapses the interior edge to the new node. Define the sheaf $L' = \pi_*(L)$ on C' , which is a line bundle because $d = 0$. Then, $h^0(C, L) = h^0(C', L')$.

Proof

Since d is zero, $H^0(C_{\text{mid}}, L|_{C_{\text{mid}}})$ is spanned by one constant section γ . Suppose that sections over C_1 (resp. C_2) is glued to sections over C_{mid} with descent data $1 \in \mathbb{C}^*$ (resp. λ). Any section $s_1 \in H^0(C_1, L|_{C_1})$ and $s_2 \in H^0(C_2, L|_{C_2})$ satisfy $s_1(p_1) = \gamma$ and $s_2(p_2) = \lambda\gamma = \lambda s_1(p_1)$. This shows that $h^0(C, L) = h^0(C', L')$. \blacksquare

3.3. Terminal graphs

Definition 3.11. We call a connected graph Γ that cannot be reduced further by our techniques (pruning external trees and removing internal edges) terminal.

3.3.1. Rational circuits

Definition 3.12. A rational circuit is a terminal graph whose components are all rational.

Example 3.13. The only rational circuit Γ with $\beta_1(\Gamma) = 0$ consists of a single vertex and no edges, i.e. is a rational curve.

Lemma 4. If Γ is a rational circuit with $1 < V$ vertices and first Betti number $\beta_1(\Gamma)$. Then

$$V \leq 2\beta_1(\Gamma) - 2. \quad (56)$$

Proof

Recall that the first Betti number of a graph is given by

$$\beta_1(\Gamma) = E + C - V, \quad (57)$$

where E is the number of edges, C the number of connected components and V the number of vertices. We assume that Γ is a rational circuit. So, by definition, Γ is connected and $C = 1$. We see that

$$E = \beta_1(\Gamma) + V - 1. \quad (58)$$

Assume that there are at least two (rational) vertices V in Γ . Such a vertex can be removed by our techniques if there are less than three edges connecting to it. Otherwise, this vertex either belongs to a tree or is an internal edge. So in order for the graph Γ to be terminal, we must have at least 3 edges connecting to each vertex:

$$\frac{3V}{2} \leq E = \beta_1(\Gamma) + V - 1. \quad (59)$$

Consequently, we conclude that for a fixed first Betti number $\beta_1(\Gamma)$, a rational circuit has a number of vertices V subject to the condition $V \leq 2\beta_1(\Gamma) - 2$. ■

Example 3.14. Let us consider rational circuits Γ with $\beta_1(\Gamma) = 1$ and $1 < V$. Then, the above bound states:

$$V \leq 2\beta_1(\Gamma) - 2 = 0. \quad (60)$$

Consequently, there are no such rational circuits. Rather, the only rational circuits Γ with $\beta_1(\Gamma) = 1$ satisfy $V = 1$ and $E = 1$. Consequently, the only rational circuit with $\beta_1(\Gamma) = 1$ is as follows:


(61)

Observe that each rational circuit Γ describes, and is determined by, a family of stable curves of arithmetic genus $\beta_1(\Gamma)$. Since the Deligne-Mumford compactified moduli space classifying stable curves of fixed genus has finitely many strata, we can conclude the following.

Corollary 3.15. The number of rational circuits with fixed first Betti number $\beta_1(\Gamma)$ is finite.

Example 3.16. For $\beta_1(\Gamma) \in \{0, 1, 2, 3\}$, the rational circuits are as follows:

- $\beta_1(\Gamma) = 0$:

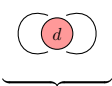


- $\beta_1(\Gamma) = 1$:

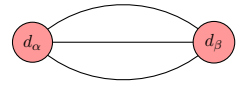


G_1

- $\beta_1(\Gamma) = 2$:



G_2

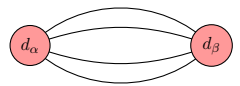
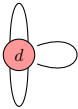


G_3

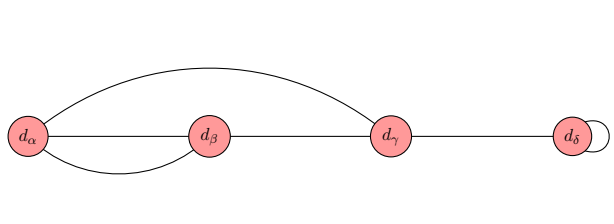
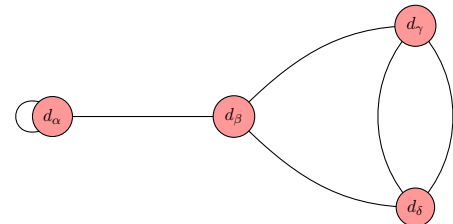
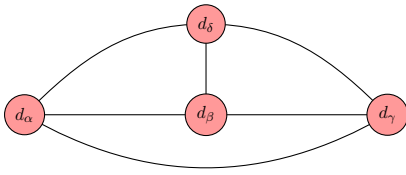
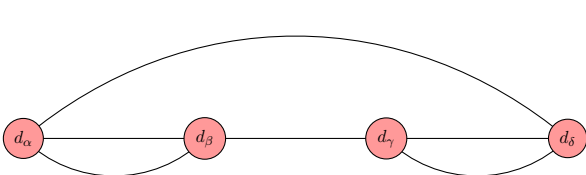
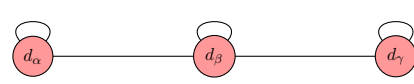
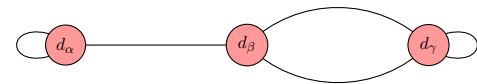
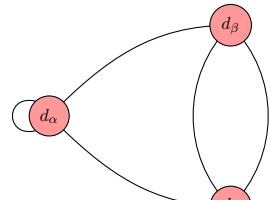
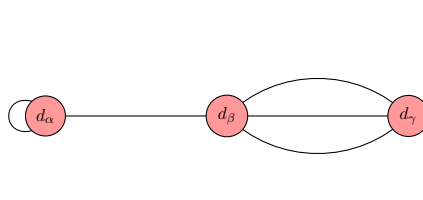
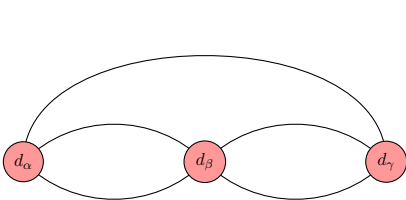
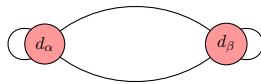
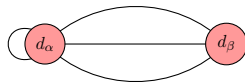


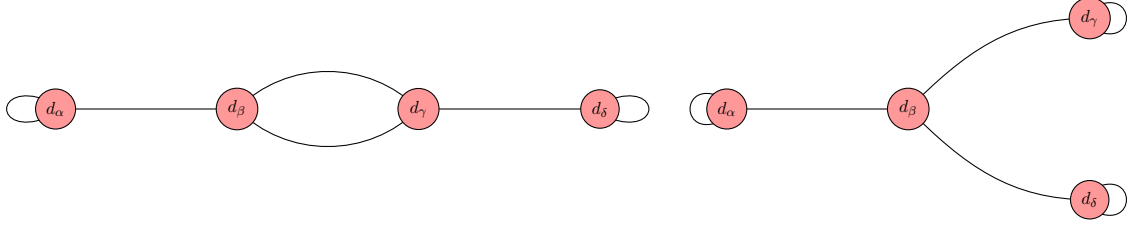
G_4

- $\beta_1(\Gamma) = 3$:



G_5





Note. A simple computer scan shows that for the QSM applications in this paper, only the graphs G_1, G_2, G_3, G_4, G_5 appear. We may thus wonder if all line bundles on these curves with the prescribed degrees have the same number of global sections, or if there are exceptions (a.k.a. jumps). For G_1 , we work out the answer below. The remaining graphs are addressed in appendix A.1.

Definition 3.17. Consider a rational circuit Γ . By definition, this is a terminal graph whose components are all rational. In addition, by our prescription, for each rational component/vertex V_i of Γ , there is an integer d_i which encodes a line bundle $L_i = \mathcal{O}_{V_i}(d_i) \cong \mathcal{O}_{\mathbb{P}^1}(d_i)$. Altogether, this defines a family \mathcal{F} of line bundles on the nodal curve C^\bullet whose dual graph is Γ , such that for every $L \in \mathcal{F}$ and every vertex V_i of Γ :

$$L|_{V_i} = L_i = \mathcal{O}_{V_i}(d_i) \cong \mathcal{O}_{\mathbb{P}^1}(d_i). \quad (62)$$

We say that Γ is non-jumping if $h^0(C^\bullet, L)$ is the same for all $L \in \mathcal{F}$. Otherwise, we say that Γ is jumping.

Remark. For our applications to the Quadrillion Standard models, we must tell under what conditions on the degree d_i , the rational circuits G_1, G_2, G_3, G_4 and G_5 are jumping.

Proposition 3.18. The rational circuit G_1 is jumping iff $d = 0$:


(63)

Proof

If $d < 0$, then $h^0(G_1, L) = 0$ for all $L \in \mathcal{F}$. Next, consider $d = 0$. Then the sections on the \mathbb{P}^1 are constant. Provided that the descent data is 1, then any constant section glues across the node and we have $h^0(G_1, L) = 1$. However, if the descent data satisfies $\lambda \neq 1$, then only the section identically zero glues across the node and $h^0(G_1, L) = 0$. So for $d = 0$, G_1 is jumping. Finally, consider $d > 0$. Pick $[x : y]$ as homogeneous coordinates of $V_1 = \mathbb{P}^1$ and position the nodes (my means of an $\mathrm{SL}(2, \mathbb{C})$ transformation) at $[1 : 0]$ and $[0 : 1]$. Then the most general section $\varphi \in H^0(V_1, L|_{V_1})$ is of the form

$$\varphi = \sum_{i=0}^d \alpha_i x^i y^{d-i}. \quad (64)$$

This section is subject to the gluing condition $\alpha_0 = \lambda \alpha_d$. Hence, $h^0(G_1, L) = d$ for all $L \in \mathcal{F}$. ■

Note. By similar arguments, one can identify exactly for what line bundle degrees G_2, G_3, G_4 and G_5 are jumping. Specifically, one finds the following:

- G_2 is jumping iff $0 \leq d \leq 2$.

- G_3 is jumping iff $0 \leq d_\alpha, d_\beta \leq 1$.
- G_4 is jumping iff one of the following applies:
 - $d_\alpha < 0$ and $d_\beta = 1$,
 - $d_\alpha = 0$ and $d_\beta \geq 0$,
 - $d_\alpha = 1$ and $d_\beta < 0$,
 - $d_\alpha \geq 0$ and $d_\beta = 0$,
 - $d_\alpha = d_\beta = 1$.
- G_5 is jumping iff $0 \leq d_\alpha, d_\beta \leq 2$.

We provide the details in appendix A.1.

Remark. We notice an interesting pattern. The canonical degree typically appears to be a sort of “tipping” points beyond which there cannot be any jumps. For a smooth curve, this is indeed the known pattern by Serre duality. However, we also see exceptions to this rule. For instance, for the graph G_4 , there is a jump for multidegree $(d, 0)$ for all $d \geq 0$. Hence, in particular for any d larger than 2, i.e. larger than the degree of the canonical bundle of a smooth curve with genus $g = 2$.

3.3.2. Elliptic circuits

Definition 3.19. We call a terminal graph with one elliptic component and otherwise only rational components, an elliptic circuit.

Note. The key difference to the previous section is that our simplification steps never remove an elliptic curve. So there is no requirement for the elliptic curve to have at least three edges leading off.

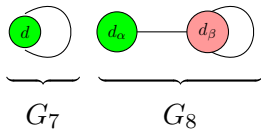
Corollary 3.20. The number of connected elliptic circuits is finite.

Example 3.21. For $\beta_1(\Gamma) \in \{0, 1, 2\}$, the connected elliptic circuits are as follows:

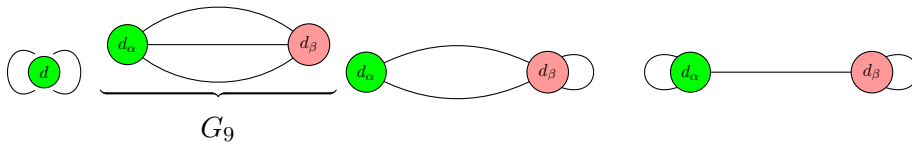
- $\beta_1(\Gamma) = 0$:

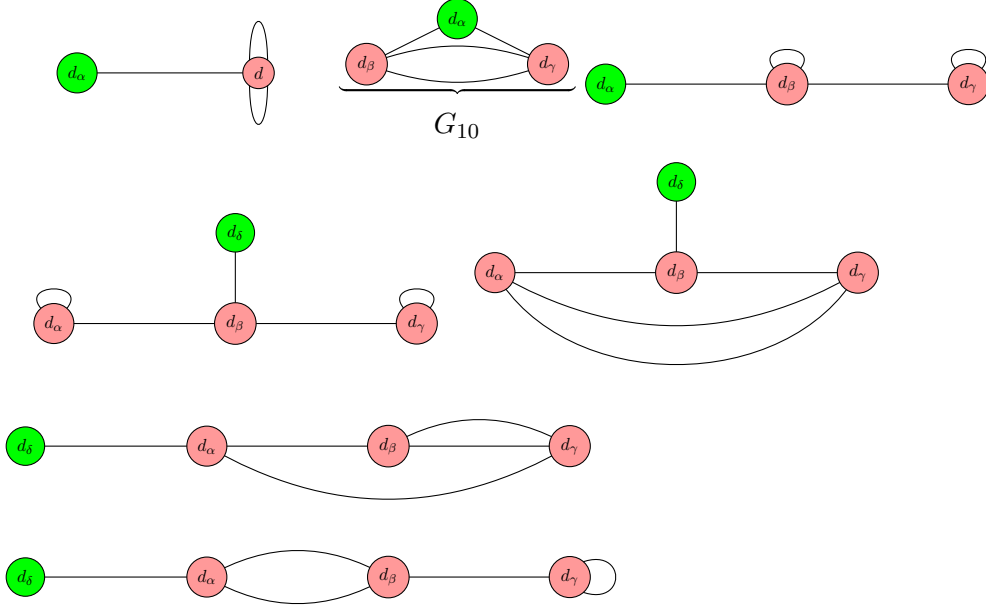


- $\beta_1(\Gamma) = 1$:



- $\beta_1(\Gamma) = 2$:





Note. A simple computer scan shows that only G_6 , G_7 , G_8 , G_9 , G_{10} appear in our QSM applications. We focus on the degrees that matter for the QSM applications and show that each configuration is jumping. For this, we construct a line bundle on the terminal graph whose number of global sections is strictly larger than the lower bound given the sum of the number of local sections minus the number of edges. The detailed arguments are given in appendix A.2.

4. Implications for F-theory QSMs

4.1. Improved statistics for “rational” QSMs

We now employ the refined simplification techniques to recompute the number of limit root bundles for the 23 QSMs whose canonical nodal quark-doublet curve consists of rational curves only. In order to fully appreciate the changes, we compare the refined results computed in this work with the results obtained with *the old techniques* [7]. We list the corresponding numbers in table 1.

We must first recall how to read these tables. First, look at the line concerning Δ_{134}° , which lists the information for the F-theory QSM family $B_3(\Delta_4^\circ)$. On the smooth, irreducible quark-doublet curve $C_{(3,2)_{1/6}}$ in this family, there are 12^8 root bundles of interest. We estimated their number of global sections from those of the 12^8 corresponding limit roots on the canonical nodal quark-doublet curve $C_{(3,2)_{1/6}}^\bullet$ in this family. In [7], we found that (roughly) 99.9952% of these 12^8 limit root bundles have exactly three global sections. Consequently, there are (roughly) 0.0048% of the limit roots left. Our techniques in [7] would only bound the number of global sections of these 0.0048% of the limit root bundles from below by three. Consequently, this fraction of the limit roots is listed in the column labeled as ≥ 3 .

At the bottom of table 1, we list the refined results computed in this work. These numbers are rounded to four decimal places. Notice that the error margins are always smaller than 0.23%, which is a stark improvement in comparison to the results in [7] or even [6].

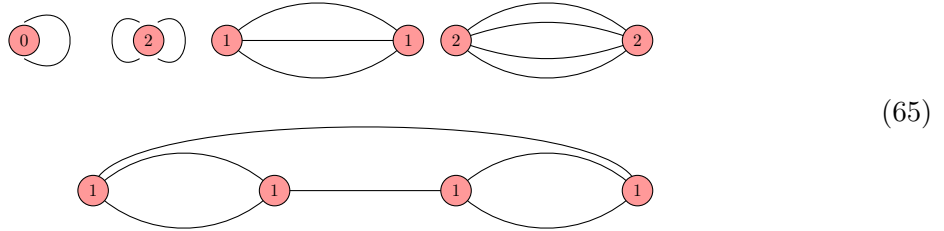
By repeating the analysis in [7], one finds that for Δ_{134}° , there is a unique setup that could not be sorted algorithmically. This configuration has the degree of the canonical bundle. By observing that the canonical bundle solves the root bundle constraint in question, [7] concludes

Polytope	$\overline{K}_{B_3}^3$	Results based on [7]						
		= 3	≥ 3	= 4	≥ 4	= 5	≥ 5	= 6
Δ_4°	6	99.9952		0.0048				
Δ_{134}°	6	99.7830	0.2170					
$\Delta_{128}^\circ, \Delta_{130}^\circ, \Delta_{136}^\circ, \Delta_{236}^\circ$	6	99.8891	0.1109					
Δ_{254}°	10	95.9365	0.5264	3.5065	0.0131	0.0175	0.0000	
Δ_{52}°	10	95.3269	0.7489	3.8812	0.0254	0.0175	0.0001	
Δ_{302}°	10	95.9225	0.5372	3.5090	0.0133	0.0181		
Δ_{786}°	10	94.8418	0.2689	4.8368	0.0100	0.0425	0.0000	
Δ_{762}°	10	94.7752	0.2785	4.8948	0.0110	0.0405	0.0000	
Δ_{417}°	10	94.8380	0.2799	4.8290	0.0102	0.0428	0.0000	0.0001
Δ_{838}°	10	94.6510	0.2798	5.0106	0.0109	0.0476	0.0001	
Δ_{782}°	10	94.6400	0.2780	5.0244	0.0115	0.0460	0.0001	
$\Delta_{377}^\circ, \Delta_{499}^\circ, \Delta_{503}^\circ$	10	93.4431	0.2416	6.2185	0.0132	0.0835	0.0001	
Δ_{1348}°	10	93.6799	0.0388	6.1970	0.0009	0.0833		0.0001
$\Delta_{882}^\circ, \Delta_{856}^\circ$	10	93.4356	0.2615	6.2051	0.0148	0.0824	0.0001	0.0005
Δ_{1340}°	10	92.2900	0.0153	7.5511	0.0005	0.1427		0.0004
Δ_{1879}°	10	92.2864	0.0260	7.5439	0.0010	0.1420		0.0007
Δ_{1384}°	10	90.8524	0.0031	8.9219	0.0001	0.2213		0.0012
		Results based on the current work						
Polytope	$\overline{K}_{B_3}^3$	= 3	≥ 3	= 4	≥ 4	= 5	≥ 5	= 6
Δ_4°	6	99.9952		0.0048				
Δ_{134}°	6	99.9952		0.0048				
$\Delta_{128}^\circ, \Delta_{130}^\circ, \Delta_{136}^\circ, \Delta_{236}^\circ$	6	99.9952		0.0048				
Δ_{254}°	10	96.3942	0.0687	3.5193	0.0003	0.0175		
Δ_{52}°	10	96.0587	0.0171	3.9066	0.0000	0.0176		
Δ_{302}°	10	96.3960	0.0636	3.5222	0.0001	0.0181		
Δ_{786}°	10	95.0714	0.0393	4.8466	0.0002	0.0425		
Δ_{762}°	10	95.0167	0.0369	4.9052	0.0005	0.0407		
Δ_{417}°	10	95.0745	0.0433	4.8389	0.0003	0.0429		0.0001
Δ_{838}°	10	94.9092	0.0215	5.0216	0.0000	0.0477		
Δ_{782}°	10	94.9019	0.0161	5.0359	0.0000	0.0461		
$\Delta_{377}^\circ, \Delta_{499}^\circ, \Delta_{503}^\circ$	10	93.6500	0.0347	6.2312	0.0005	0.0836		
Δ_{1348}°	10	93.7075	0.0112	6.1978	0.0001	0.0833		0.0001
$\Delta_{882}^\circ, \Delta_{856}^\circ$	10	93.6546	0.0425	6.2190	0.0009	0.0825		0.0005
Δ_{1340}°	10	92.2989	0.0064	7.5515	0.0001	0.1427		0.0004
Δ_{1879}°	10	92.3015	0.0108	7.5447	0.0002	0.1421		0.0007
Δ_{1384}°	10	90.8524	0.0031	8.9219	0.0001	0.2213		0.0012

Table 1: We compare the Brill-Noether numbers computed in [7] with the refined results of the current work. The results are rounded to four decimal places.

that this configuration does indeed correspond to the canonical bundle and admits four global sections. With the exception of Δ_8° , whose canonical nodal quark-doublet curve admits an elliptic component, one can repeat this argument for all remaining setups with $\overline{K}_{B_3}^3 = 6$. This leads to the results listed in table 1.

Crucially, note that this argument cannot be repeated for setups with $\overline{K}_{B_3}^3 = 10$; essentially because we then have to solve a root bundle constraint which does not admit the canonical bundle as solution. Still, our results are optimal in a certain sense. The list of terminal graphs for which our improved computer scan [77] could only compute a lower bound on the number of global sections is as follows:



We argued in appendix A.1, that all of these terminal circuits are jumping. In other words, the number of global sections depends on the descent data. As our computer scan [77] is (at least of now) not being provided with that information, it derives the best possible answer based on the combinatoric data provided.

4.2. Improved statistics for “elliptic” QSMs

Our advanced techniques help to improve the results for the QSM with a single elliptic curve. Since most of the remaining ignorance in the previous work [7] originates from trees with an elliptic component. So we expect a massive improvement. As an example, let us look at Δ_{88}° . The Brill-Noether table obtained from application of our *old techniques* in [7] and its refined counterpart based on the techniques presented in this work are displayed in table 2.

We first recall the notation in this table. We have analyzed 20^{12} limit root bundles on the canonical quark-doublet curve $C_{(3,2)_{1/6}}^\bullet$ in the F-theory QSM-family $B_3(\Delta_{88}^\circ)$. Those limit roots are described by line bundles on a (possibly nodal) curve that is obtained from blowing up $0 \leq N \leq 6$ nodes of $C_{(3,2)_{1/6}}^\bullet$. For fixed N , only a fraction of the 20^{12} limit roots are obtained. We have enumerated them all and made an effort to compute their number of global sections. For instance, in [7], we found that for $N = 0$, there are 781 680 888 limit root bundles with exactly three global sections.² You find this number at the top-left of table 2. Similarly, we encountered 62 712 limit root bundles for $N = 0$, for which we could only compute a lower bound on the number of global sections in [7]. Namely, we found that the number of global sections is bounded below by three. Hence, you find this number 62 712 at the top row with $N = 0$ and column with ≥ 3 . We regard this number of limit root bundles for which we could not uniquely determine the number of global sections as an ignorance to our analysis. Finally, the row beginning by Σ lists the sum of all limit root bundles with $0 \leq N \leq 6$ and certain (lower bound on the) number of global sections. For instance, there is a total of 31 563 200 limit root bundles with exactly four global sections in [7].

²More precisely, there are actually $781\,680\,888 \times 20^5$ such limit roots. However, all counts in this table are multiples of the geometric multiplicity $\mu = 20^5$. For ease of presentation and in agreement with [7], we omit the factor 20^5 .

Results based on [7]						
N	$= 3$	≥ 3	$= 4$	≥ 4	$= 5$	≥ 5
0	781 680 888	62 712	25 196 800	0	106 800	0
1	163 221 088	206 886 912	5 967 200	5 200 000	0	7 200
2	13 270 504	66 014 696	399 200	1 355 600	0	0
3	504 800	9 318 400	0	88 800	0	0
4	4 400	687 600	0	0	0	0
5	0	24 800	0	0	0	0
6	0	1 600	0	0	0	0
Σ	958 681 680	282 996 720	31 563 200	6 644 400	106 800	7 200

Results based on the current work						
N	$= 3$	≥ 3	$= 4$	≥ 4	$= 5$	≥ 5
0	781 680 888	62 712	25 196 800	0	106 800	0
1	366 819 888	3 288 112	11 167 200	0	7 200	0
2	76 851 304	2 433 896	1 694 800	60 000	0	0
3	8 250 400	1 572 800	64 800	24 000	0	0
4	362 000	330 000	0	0	0	0
5	0	24 800	0	0	0	0
6	0	1 600	0	0	0	0
Σ	1 233 964 480	7 713 920	38 123 600	84 000	114 000	0

Table 2: The Brill-Noether table computed for Δ_{88}° in [7] (top) and its refined counterpart based on the current work (bottom). Those numbers are listed as multiples of the geometric multiplicity μ , which happens to be 20^5 for Δ_{88}° .

Let us now compare this Brill-Noether table from [7] with the results obtained from our *refined techniques*. This improved answer is listed at the bottom of table 2. Hence, with the techniques in [7] we found the lower bound three to the number of global sections of 282 996 720 limit root bundles, whereas this happened for merely 7 713 920 limit roots once our advanced techniques were employed. This is a drastic reduction of ignorance! It is enlightening to express the two Σ -rows in percentages of the 20^{12} limit root bundles:

	$= 3$	≥ 3	$= 4$	≥ 4	$= 5$	≥ 5
Σ in [7]	74.8970	22.1091	2.4659	0.5191	0.0083	0.0006
Σ in current work	96.4034	0.6027	2.9784	0.0066	0.0089	

(66)

So the total ignorance dropped from about 22.7% to about 0.7%. Clearly, this is a stark improvement! Indeed, this finding applies more generally to the 10 families of elliptic F-theory QSMs that we analyze in this work. We provide the comparison among the results from [7] and the refined answers computed in this work in table 3. While we definitely reduced the ignorances significantly, let us emphasize that these results are optimal in a certain sense. Namely, we can easily list all setups for which our computer algorithm could only compute a lower bound on the number of global sections. Then, we can analyze what it would take to turn these lower bounds into exact counts of global sections. For instance, the remaining computation for Δ_8° concerns

Polytope	$\overline{K}_{B_3}^3$	Results based on [7]					
		= 3	≥ 3	= 4	≥ 4	= 5	≥ 5
Δ_8°	6	76.3889	23.6111				
Δ_{88}°	10	74.8970	22.1091	2.4659	0.5191	0.0083	0.0006
Δ_{110}°	10	82.3757	14.1284	3.100	0.3827	0.0132	
$\Delta_{272}^\circ, \Delta_{274}^\circ$	10	78.0509	18.0470	3.3587	0.5255	0.0155	0.0024
Δ_{387}°	10	73.8375	21.9358	3.5044	0.6900	0.0295	0.0028
$\Delta_{798}^\circ, \Delta_{808}^\circ, \Delta_{810}^\circ, \Delta_{812}^\circ$	10	76.9517	17.8638	4.4362	0.6972	0.0468	0.0043

Polytope	$\overline{K}_{B_3}^3$	Results based on the current work					
		3	≥ 3	4	≥ 4	5	≥ 5
Δ_8°	6	99.9421		0.0579			
Δ_{88}°	10	96.4034	0.6027	2.9784	0.0066	0.0089	
Δ_{110}°	10	95.5794	0.8846	3.5170	0.0059	0.0131	
$\Delta_{272}^\circ, \Delta_{274}^\circ$	10	95.3336	0.6916	3.9450	0.0118	0.0180	
Δ_{387}°	10	95.1545	0.5358	4.2769	0.0005	0.0323	
$\Delta_{798}^\circ, \Delta_{808}^\circ, \Delta_{810}^\circ, \Delta_{812}^\circ$	10	93.8212	0.8852	5.2384	0.0034	0.0518	

Table 3: We compare the Brill-Noether numbers computed in [7] with the refined results of the current work. The results are rounded to four decimal places.

(a family of) line bundles of the canonical degree. In fact, we could argue implicitly that these must be the canonical bundle [7]. However, purely based on the combinatorics data that the computer uses, it is impossible to arrive at that conclusion. Rather, the descent data of the limit root bundles is needed. Hence, based on the information provided by the current computer scan, this result cannot be improved. Likewise, for the remaining QSM geometries in the above table, the remaining computations concern one or multiple of the following configurations:

$$(67)$$

All of these are jumping terminal graphs, which were derived in appendix A.1 and appendix A.2. To tell the number of global sections precisely, one needs the descent data and/or the exact line bundle divisor on the elliptic curve. So based on the currently available combinatoric data for our computer scan, the above results are fully optimized.

4.3. Absence of vector-like quark-doublets

Let us summarize our findings regarding the analyzed 33 families of F-theory QSMs:

Polytope	$\overline{K}_{B_3}^3$	$P_{(3)}$	N_{roots}	\check{N}_{FRST}	\hat{N}_{FRST}
Δ_8°	6	99.9421	12^8	3.867×10^{13}	2.828×10^{16}
Δ_4°	6	99.9952	12^8	3.188×10^{11}	
Δ_{134}°	6	99.9952	12^8	7.538×10^{10}	
$\Delta_{128}^\circ, \Delta_{130}^\circ, \Delta_{136}^\circ, \Delta_{236}^\circ$	6	99.9952	12^8	3.217×10^{11}	
Δ_{88}°	10	96.4034	20^{12}	5.231×10^{10}	1.246×10^{14}
Δ_{110}°	10	95.5794	20^{12}	5.239×10^8	
$\Delta_{272}^\circ, \Delta_{274}^\circ$	10	95.3336	20^{12}	3.212×10^{12}	2.481×10^{15}
Δ_{387}°	10	95.1545	20^{12}	6.322×10^{10}	6.790×10^{12}
$\Delta_{798}^\circ, \Delta_{808}^\circ, \Delta_{810}^\circ, \Delta_{812}^\circ$	10	93.8212	20^{12}	1.672×10^{10}	2.515×10^{13}
Δ_{254}°	10	96.3942	20^{12}	1.568×10^{10}	
Δ_{52}°	10	96.0587	20^{12}	1.248×10^8	
Δ_{302}°	10	96.3960	20^{12}	5.750×10^7	
Δ_{786}°	10	95.0714	20^{12}	9.810×10^8	
Δ_{762}°	10	95.0167	20^{12}	1.087×10^{11}	2.854×10^{13}
Δ_{417}°	10	95.0745	20^{12}	1.603×10^9	
Δ_{838}°	10	94.9092	20^{12}	4.461×10^9	
Δ_{782}°	10	94.9019	20^{12}	3.684×10^9	
$\Delta_{377}^\circ, \Delta_{499}^\circ, \Delta_{503}^\circ$	10	93.6500	20^{12}	4.461×10^9	
Δ_{1348}°	10	93.7075	20^{12}	4.285×10^9	
$\Delta_{882}^\circ, \Delta_{856}^\circ$	10	93.6546	20^{12}	3.180×10^9	
Δ_{1340}°	10	92.2989	20^{12}	4.496×10^9	
Δ_{1879}°	10	92.3015	20^{12}	4.461×10^9	
Δ_{1384}°	10	90.8524	20^{12}	7.040×10^9	

Recall that these geometries are one-to-one to fine, regular, star triangulations (FRSTs) of reflexive 3-dimensional polytopes. Some of these polytopes are very complicated and the number of triangulations can only be estimated [71]. In the last two columns, we have listed the known lower and upper bounds to the number of FRSTs. If the exact number of FRSTs is known, we have not listed an upper bound \hat{N}_{FRST} as we hope that this helps to read this table.

Let us analyze these numbers. A natural question is to consider the union of all 33 families of F-theory QSMs and then to ask how likely it is to find no vector-like exotics on the quark-doublet curve. In other words, if we throw a dart at the board of all these QSM families, how likely it is that we hit a configuration without vector-like exotics on the quark-doublet curve? To this end, we focus on the quantity

$$P = \frac{\sum_{i \in I} P_{(3)}^{(i)} \cdot N_{\text{roots}}^{(i)} \cdot N_{\text{FRST}}^{(i)}}{\sum_{i \in I} N_{\text{roots}}^{(i)} \cdot N_{\text{FRST}}^{(i)}}, \quad (69)$$

where I is the indexing set of the polytopes in the above table. The complicating fact is that we cannot uniquely tell the number of FRSTs for 10 polytopes. Rather, for these polytopes we

only know a lower and upper bound to the number of triangulations [71]. So what we do, is we minimize this quantity in the domain of the admissible triangulations. This task can easily be completed e.g. with `Mathematica` [79]³. We find that the likeliness for exactly three global sections on the quark doublet curve is at least 93.91%. This minimum percentage is attained by maximizing the number of FRSTs for Δ_{798}° and minimizing the number of all other FRSTs.

In principle one could be tempted to repeat this analysis to also find an upper bound. Such a naive approach would use the sum of the percentage of roots with exactly three sections and that of roots for which we could only bound the number of global sections below by three. The outcome of this computation is then 96.96% – attained by maximizing the number of FRSTs for Δ_8° , Δ_{88}° and minimizing the number of all other FRSTs. Note however, that we actually want to count global sections of root bundles on the physical quark-doublet curve and not the nodal curves, for which we execute the computations presented in this work. Along the smoothing $C_{(\mathbf{3},\mathbf{2})_{1/6}}^\bullet \rightarrow C_{(\mathbf{3},\mathbf{2})_{1/6}}$ we may lose vector-like pairs/global sections. Indeed, we cannot rule out the possibility that all root bundles may drop down to having exactly three global sections after this smoothing. This effect is not taken into account by the naive upper bound 96.96%, which must therefore be discarded.

A complementary answer is obtained by estimating the chances for exactly one vector-like exotic on the nodal quark-doublet curve $C_{(\mathbf{3},\mathbf{2})_{1/6}}^\bullet$. It is important to recall that we want to estimate this number on the original smooth matter curves. Due to the deformation process from the nodal to the smooth, irreducible curves, we can merely provide an upper bound from our estimates on the nodal curve. The latter is readily obtained with e.g. `Mathematica` [79], namely the chances for this are at most 5.17%. This maximal value is obtained for a maximal number of FRSTs for Δ_{798}° and minimal number of FRSTs for all other polytopes.

5. Summary and outlook

The geometries of the Quadrillion F-theory Standard Models (QSMs) [4] are defined by toric 3-folds, which arise from full, regular, star triangulations of certain polytopes in the Kreuzer-Skarke list of 3-dimensional reflexive polytopes [70]. The vector-like spectra in QSM geometries are given by the cohomologies of certain roots $P_{\mathbf{R}}$ (twists of certain powers of) the canonical bundle on the matter curve $C_{\mathbf{R}}$ [5]. These roots are not unique, and it is unclear which ones come from F-theory gauge potentials in the Deligne cohomology. Investigating this matter is currently beyond our abilities, so [5–7] analyzed *all* mathematically possible root bundles, including those that could be induced from the G_4 -flux. They conducted a local and bottom-up analysis, dealing with one matter curve at a time and neglecting any correlations among the vector-like spectra on different matter curves.

Counting root bundles on $C_{\mathbf{R}}$ becomes easier when the matter curve is deformed into a nodal curve. Constructing root bundles on smooth curves is challenging, but on nodal curves, it amounts to using the combinatorics of limit roots [69]. Additionally, for each family $B_3(\Delta^\circ)$ of F-theory QSMs, there is a canonical nodal curve $C_{\mathbf{R}}^\bullet$ that depends solely on Δ° [6]. Therefore, the vector-like spectra for the entire family $B_3(\Delta^\circ)$ can be estimated with a single calculation by studying the limit roots on this nodal curve $C_{\mathbf{R}}^\bullet$.

After deformation, we turn to counting limit root bundles with a specific number of global sections. This was the main goal of [7], which focused on the family $B_3(\Delta_4^\circ)$ of $\mathcal{O}(10^{11})$ F-theory QSMs. The majority of the limit roots were defined over tree-like rational curves, and their

³One can also work out this result with the *Karush–Kuhn–Tucker* conditions [80, 81], which generalize the method of Lagrange multiplier. The key step is to employ the complementary slackness conditions.

line bundle cohomologies were computed using an algorithm that simplified a line bundle on a tree-like nodal curve without changing the number of global sections. The remaining limit roots were defined over circuit-like curves, and their cohomologies were counted manually. Fortunately, there were only a few of them, namely five for the $B_3(\Delta_4^\circ)$ family, because the involved nodal curves had relatively small Betti numbers and high root indices. On four of the curves, the line bundles were found to have exactly three sections. On the remaining curve, labeled as a *jumping circuit* in [7], the line bundle was identified as the canonical bundle, which has as many sections as the arithmetic genus, namely four in this case. This is why at least 99.995% of limit root bundles on the nodal curves $C_{(3,2)_{1/6}}^\bullet$, $C_{(\bar{3},1)_{-2/3}}^\bullet$, and $C_{(1,1)_1}^\bullet$ have exactly three global sections within the F-theory QSMs of the family $B_3(\Delta_4^\circ)$.

This paper seeks to upgrade the results of [7] in two ways. First, it develops a systematic algorithm that determines line bundle cohomologies on circuit-like curves with rational and elliptic components. Previously, this was done manually in [7]. We present two techniques that simplify the dual graphs of nodal curves: the removal of subtrees in section 3.1 and the removal of interior edges in section 3.2. These simplifications result in a finite number of so-called terminal circuits, which are graphs that cannot be further reduced. The terminal graphs were classified in section 3.3, and their line bundle cohomologies were examined case-by-case. The relevant computations can be found in section 3.3 as well as appendix A.1, appendix A.2. Like in [7], some circuits were found to be jumping depending on the descent data, and only a lower bound on the number of global sections can be obtained in these cases.

With this established algorithm, this paper seeks to move beyond the family $B_3(\Delta_4^\circ)$ and widen the scope of analysis. The simplification algorithm was applied to 33 distinct QSM families to assess the probability of no vector-like exotics. The improved statistics can be found in section 4, where table 1 and table 3 compare our current findings with those obtained using old techniques from [7]. As expected, this algorithm improved our ability to conclusively determine line bundle cohomology and helped decrease the statistical ignorance from previous papers. For instance, the total ignorance for elliptic circuits within the family $B_3(\Delta_{88}^\circ)$ dropped from 22.7% to 0.7%, a massive upgrade. These results are optimal in the sense that pure combinatorics alone will not offer any more improvement. Further progress requires deeper knowledge of the descent data and the line bundle divisor on elliptic curves.

In section 4.3, we discovered that the probability of having precisely three global sections on the quark doublet curve is at least 93.91%. Although this value is lower than the previous probability of 99.995% mentioned in [7], there is a crucial distinction. In our analysis, we encompass multiple QSM families, whereas [7] only examined a single QSM family. Hence, our current estimation of 93.91% provides a more comprehensive representation of the likelihood of lacking vector-like exotics on the quark-doublet curve across the majority of QSM setups. It is important to emphasize that 93.91% serves as a lower bound. For certain QSM families, the exact number of elements remains unknown. Stated differently, for some of the 3-dimensional reflexive polytopes in the Kreuzer-Skarke list [70] the exact number of fine regular star triangulations is unknown. Only lower and upper bounds for the number of fine regular star triangulations are known [71]. We minimized the absence of vector-like exotics within the domain formed from these lower and upper bounds on triangulations. The stated minimum of 93.91% is attained for minimal number of FRSTs for polytopes with a high probability of lacking vector-like exotics and maximized the number of FRSTs for polytopes with a (relatively) low probability of lacking vector-like exotics. The latter specifically pertains to the $B_3(\Delta_{272}^\circ)$ and $B_3(\Delta_{274}^\circ)$ families.

It should be noted that only 33 families of QSMs were studied, leaving 675 families remaining. While each comes with only few triangulations, the number of roots grows exponentially. The

number of roots is given by

$$\left(2\overline{K}_{B_3}^3\right)^{2g}, \quad g = \frac{2 + \overline{K}_{B_3}^3}{2}: \text{ the genus of the quark-doublet curve.} \quad (70)$$

Hence, the cases $\overline{K}_{B_3}^3 = 18$ and $\overline{K}_{B_3}^3 = 30$, which have not been covered in this paper, come with 36^{10} and 60^{16} roots each. These numbers are huge compared to the setups in our analysis. However, since these cases did not our statistically rooted top-down condition, $h^{2,1}(\widehat{Y}_4) \geq g$ where g is the genus of $C_{(3,2)_{1/6}}$ [6], they were discarded.⁴ Nevertheless, based on the number of (root bundle) configurations that they provide and the fact that large \overline{K}^3 corresponds to small $h^{1,1}(\widehat{Y}_4)$, which is needed for "realistic volumes" of the gauge divisors $V(s_3)$, $V(s_9)$ in stretched Kaehler cones [82], one should study these setups eventually.

This work also does not address the fundamental question of understanding which root bundles are induced by F-theory gauge potentials in the Deligne cohomology. We refer the reader to [5] to see how the G_4 -flux quantization condition discussed in [83] gives rise to root bundles. One possible scenario is for all physically allowed gauge potentials to induce only a subset of limit roots on one matter curve. Another scenario is for the fluxes to induce a specific root on one matter curve but induce a few roots on another. To study this complex question, one can begin by setting $G_4 = 0$ and studying the origins of the root bundles in Deligne cohomology. In this setting, the root bundles are spin bundles, and so we seek to answer which spin bundles on the matter curve are compatible with the geometry of the F-theory compactification. For instance, an important condition from the physics is the cancellation of the Freed-Witten anomaly [84]. A complete answer to all of this requires detailed investigation, similar to the steps outlined in [85]. One could also investigate the relationship between these spin bundles and the appearance of one half of the second Chern class (of the tangent bundle of \widehat{Y}_4) in the G_4 -flux quantization condition [83]. Although our findings state that at least 93.91% of limit roots have exactly three global sections, we cannot get a definitive answer regarding the absence of vector-like exotics until this matter is resolved. A detailed examination of such top-down conditions is planned for future research.

We eventually want to study the absence of vector-like exotics on the Higgs curve. However, this involves overcoming some computational challenges. Due to the Higgs curve having high genus and a large number of components, we will end up with a rather complicated curve even after simplification. The root bundle constraint is also different, and we will have to analyze a much larger number of roots. Nevertheless, our newfound techniques may uncover some structure that is not apparent yet. A more general extension could focus on other Standard Model setups, such as those considered in [34, 39, 41, 44, 45], and investigate these constructions with the techniques presented in this work. We reserve these studies for future work.

This paper, and in particular table 1 and table 3, should be seen as a computational approximation to describing the Brill-Noether Theory of root bundles on nodal curves. Such a theory is underdeveloped in the mathematical literature. These arithmetic perspectives may encourage more robust theorems to be made in the future. For instance, one may gain more insight by studying the descent data underlying limit root bundles and its behavior under deformation in [69]. As a common technique used in Brill-Noether theory, the application of limit linear series to limit root bundles is also compelling [86, 87]. It would be interesting to compare the phenomena observed in our investigation to classical Brill-Noether theory. In particular, some circuits

⁴4 setups were discarded even though they satisfied $h^{2,1}(\widehat{Y}_4) \geq g$, but their canonical nodal quark doublet curve $C_{(3,2)_{1/6}}^\bullet$ have an irreducible component of genus strictly larger than 1.

exhibit jumping behavior, which seems to resemble Brill-Noether jumps on smooth irreducible curves.

To conclude, one potential application in machine learning is to study and detect patterns linking the graphs to the corresponding Brill-Noether approximations. In the past, for many line bundles on nodal curves with relatively simple dual graphs, our computed Brill-Noether numbers featured a high ignorance in the numbers of global sections. Thus, the data was insufficient to learn conclusive results from. Now that we have improved our computational capabilities, we anticipate that most of this ignorance can be removed and, based on this refined data, a much better trained algorithm can be obtained. This algorithm could then either be used to estimate the number of global sections on the Higgs curve or in an attempt to predict a mathematical theorem underlying the Brill-Noether theory of root bundles on nodal curves.

Acknowledgements

The OSCAR computer algebra system was used for key computations in this work. The reliable computations conducted by the supercomputer `plesken.mathematik.uni-siegen.de` allowed us to count limit root bundles. This we truly appreciate. M. B. expresses gratitude towards his colleague Tobias Metzloff for valuable discussions. The work of M. B. was supported by the SFB-TRR 195 *Symbolic Tools in Mathematics and their Application* of the German Research Foundation (DFG) and the Forschungsinitiative des Landes Rheinland-Pfalz through *SymbTools – Symbolic Tools in Mathematics and their Application*. The work of M.C. is supported by DOE Award DE-SC0013528Y and the Simons Foundation Collaboration grant #724069 on “Special Holonomy in Geometry, Analysis and Physics”. M.C. thanks the Slovenian Research Agency No. P1-0306 and the Fay R. and Eugene L. Langberg Chair for support. R.D. and M.O. are partially supported by the NSF grant DMS 2001673 and by the Simons Foundation Collaboration grant #390287 on “Homological Mirror Symmetry”. M.O. is grateful for the support by the Ph.D. Presidential Fellowship research fund.

Let us take $\lambda_1 = \frac{1}{2}$, $\lambda_2 = 2$ and $p = \frac{1}{2}$. Then, these conditions are satisfied for all $\alpha_1, \alpha_2 \in \mathbb{C}$ and so $h^0(G_2, L) = 2$. However, for generic $\lambda_1, \lambda_2 \in \mathbb{C}^*$ and $p \in \mathbb{C} \setminus \{0, 1\}$, we have two non-trivial conditions and so $h^0(G_2, L) = 1$. Hence, G_2 is jumping for $d = 2$. Finally, focus on $d > 2$. Then the gluing conditions are

$$\alpha_0 = \lambda_1 \cdot \alpha_d, \quad (78)$$

$$\alpha_d \cdot \left[\lambda_1 + 1 - \lambda_1 \lambda_2 - \lambda_2 p^d \right] = \alpha_1 (\lambda_2 p - 1) + \alpha_2 (\lambda_2 p^2 - 1) + \sum_{i=3}^{d-1} \alpha_i \cdot (\lambda_2 p^i - 1). \quad (79)$$

Let us assume that $\lambda_2 p - 1 \neq 0$. Then, these conditions are equivalent to

$$\alpha_0 = \lambda_1 \cdot \alpha_d, \quad (80)$$

$$\alpha_1 = \frac{\alpha_d \cdot \left[\lambda_1 + 1 - \lambda_1 \lambda_2 - \lambda_2 p^d \right] - \alpha_2 (\lambda_2 p^2 - 1) - \sum_{i=3}^{d-1} \alpha_i \cdot (\lambda_2 p^i - 1)}{\lambda_2 p - 1}. \quad (81)$$

Hence, we then find $h^0(G_2, L) = d - 1$. Conversely, assume that $\lambda_2 p - 1 = 0$, i.e. $p = \frac{1}{\lambda_2}$. Recall that we must have $p \in \mathbb{C} \setminus \{0, 1\}$, so $\lambda_2 \neq 1$. In particular $\frac{1}{\lambda_2} - 1 \neq 0$. Under these assumptions, the above conditions becomes

$$\alpha_0 = \lambda_1 \cdot \alpha_d, \quad (82)$$

$$\alpha_d \cdot \left[\lambda_1 + 1 - \lambda_1 \lambda_2 - \lambda_2^{-d+1} \right] = \alpha_2 \left(\frac{1}{\lambda_2} - 1 \right) + \sum_{i=3}^{d-1} \alpha_i \cdot (\lambda_2^{-i+1} - 1). \quad (83)$$

Equivalently, we can write

$$\alpha_0 = \lambda_1 \cdot \alpha_d, \quad (84)$$

$$\alpha_2 = \frac{\alpha_d \cdot \left[\lambda_1 + 1 - \lambda_1 \lambda_2 - \lambda_2^{-d+1} \right] - \sum_{i=3}^{d-1} \alpha_i \cdot (\lambda_2^{-i+1} - 1)}{\frac{1}{\lambda_2} - 1}. \quad (85)$$

And so, again we find $h^0(G_2, L) = d - 1$. Hence, $h^0(G_2, L) = d - 1$ for all $L \in \mathcal{F}$ for $d > 2$, i.e. G_2 is non-jumping for $d > 2$. \blacksquare

Proposition A.2. G_3 is jumping iff $0 \leq d_\alpha, d_\beta \leq 1$:



Proof

First, if $d_\alpha, d_\beta < 0$, then $h^0(G_3, L) = 0$ for all $L \in \mathcal{F}$. So G_3 is non-jumping for $d_\alpha, d_\beta < 0$.

Before we proceed, let us fix some notation. We use homogeneous coordinates $[x : y]$ for $V_1 = \mathbb{P}_\alpha^1$ and $[u : v]$ for $V_2 = \mathbb{P}_\beta^1$. In terms of these, we can express the most general section $\varphi_\alpha \in H^0(V_1, L|_{V_1})$ and $\varphi_\beta \in H^0(V_2, L|_{V_2})$ as follows:

$$\varphi_\alpha = \sum_{i=0}^{d_\alpha} a_i x^i y^{d_\alpha - i}, \quad \varphi_\beta = \sum_{i=0}^{d_\beta} b_i u^i v^{d_\beta - i}. \quad (87)$$

By an $\mathrm{SL}(2, \mathbb{C})$ transformation, we can assume that the nodes are positioned at $n_1 = [1 : 0]$, $n_2 = [0 : 1]$ and $n_3 = [1 : 1]$. First, let us study situations with $d_\alpha < 0$ and $d_\beta \geq 0$. Then the gluing conditions are as follows:

$$0 = \lambda_1 b_{d_\beta}, \quad 0 = \lambda_0 b_0, \quad 0 = \sum_{i=0}^{d_\beta} b_i. \quad (88)$$

Consequently, $h^0(G_3, L) = \max\{d_\beta - 2, 0\}$ for all $L \in \mathcal{F}$, i.e. G_3 is non-jumping. Next, focus on $d_\alpha, d_\beta \geq 0$. Then, the gluing conditions are as follows:

$$a_{d_\alpha} = \lambda_1 b_{d_\beta}, \quad a_0 = \lambda_0 b_0, \quad (\lambda_1 - 1) b_{d_\beta} + (\lambda_0 - 1) b_0 = \sum_{i=1}^{d_\beta-1} b_i - \sum_{i=1}^{d_\alpha-1} a_i. \quad (89)$$

The first two conditions are never trivial. However, the third condition is trivial iff $\lambda_0 = \lambda_1 = 1$ and $0 \leq d_\alpha, d_\beta \leq 1$. Consequently, G_3 is jumping iff $0 \leq d_\alpha, d_\beta \leq 1$. \blacksquare

Proposition A.3. G_4 is jumping iff one of the following applies:

- $d_\alpha < 0$ and $d_\beta = 1$,
- $d_\alpha = 0$ and $d_\beta \geq 0$,
- $d_\alpha = 1$ and $d_\beta < 0$,
- $d_\alpha \geq 0$ and $d_\beta = 0$,
- $d_\alpha = d_\beta = 1$.



$$(89)$$

Proof

Certainly, for $d_\alpha, d_\beta < 0$ we have $h^0(G_4, L) = 0$ for all $L \in \mathcal{F}$. So for both degrees negative, G_4 is non-jumping.

We use homogeneous coordinates $[x : y]$ on $V_1 = \mathbb{P}_\alpha^1$ and $[u : v]$ on $V_2 = \mathbb{P}_\beta^1$. Fix the node positions to $[1 : 0]$, $[0 : 1]$ and $[1 : 1]$ by an $\mathrm{SL}(2, \mathbb{C})$ transformation. The node linking \mathbb{P}_α^1 and \mathbb{P}_β^1 has homogeneous coordinates $[1 : 1]$ on both V_1 and V_2 . With that being said, we can express $\varphi_\alpha \in H^0(V_1, L|_{V_1})$ and $\varphi_\beta \in H^0(V_1, L|_{V_2})$ as follows:

$$\varphi_\alpha = \sum_{i=0}^{d_\alpha} a_i x^i y^{d_\alpha-i}, \quad \varphi_\beta = \sum_{i=0}^{d_\beta} b_i u^i v^{d_\beta-i}. \quad (91)$$

On the self-edges, we enforce descent data λ_α and λ_β . We begin by analyzing mixed signs for the line bundle degrees.

- $d_\alpha < 0$ and $d_\beta = 0$:

Then, the gluing conditions are:

$$0 = \lambda_\alpha \cdot 0, \quad b_0 = \lambda_\beta \cdot b_0, \quad 0 = b_0. \quad (92)$$

So $h^0(G_4, L) = 0$ for all $L \in \mathcal{F}$, i.e. G_4 is non-jumping.

- $d_\alpha < 0$ and $d_\beta = 1$:

Then, the gluing conditions are:

$$0 = \lambda_\alpha \cdot 0, \quad b_0 = \lambda_\beta \cdot b_1, \quad 0 = b_1 \cdot (1 + \lambda_\beta). \quad (93)$$

Hence, if $\lambda_\beta = -1$, then $h^0(G_4, L) = 1$. However, for $\lambda_\beta \neq -1$, we have $h^0(G_4, L) = 0$. So G_4 is jumping for $d_\alpha < 0$ and $d_\beta = 1$.

- $d_\alpha < 0$ and $d_\beta > 1$:

Then, the gluing conditions are:

$$0 = \lambda_\alpha \cdot 0, \quad b_0 = \lambda_\beta \cdot b_{d_\beta}, \quad b_1 = -b_{d_\beta} \cdot (1 + \lambda_\beta) - \sum_{i=2}^{d_\beta-1} b_i. \quad (94)$$

So in this case, we have $h^0(G_4, L) = d_\beta - 1$ for all $L \in \mathcal{F}$ and G_4 is non-jumping.

Next, we focus on situations with $d_\alpha = 0$ and $d_\beta \geq 0$.

- $d_\alpha = d_\beta = 0$:

Then the gluing conditions are as follows:

$$a_0 = \lambda_\alpha a_0, \quad b_0 = \lambda_\beta b_0, \quad a_0 = b_0. \quad (95)$$

For generic $\lambda_\alpha, \lambda_\beta \in \mathbb{C}^*$, the only solution to these equations is $a_0 = b_0 = 0$ and hence $h^0(G_4, L) = 0$. However, if $\lambda_\alpha = \lambda_\beta = 1$, then $a_0 = b_0$ solves these conditions and $h^0(G_4, L) = 1$. Hence, G_4 is jumping for $d_\alpha = d_\beta = 0$.

- $d_\alpha = 0$ and $d_\beta > 0$:

Then, the gluing conditions are as follows:

$$a_0 = \lambda_\alpha a_0, \quad b_0 = \lambda_\beta b_{d_\beta}, \quad b_{d_\beta} \cdot (1 + \lambda_\beta) = a_0 - \sum_{i=1}^{d_\beta-1} b_i. \quad (96)$$

For generic λ_α and λ_β , we must have $a_0 = 0$ and $1 + \lambda_\beta \neq 0$. This then means that the only solution to these conditions is then given by

$$a_0 = 0, \quad b_0 = \lambda_\beta b_{d_\beta}, \quad b_{d_\beta} = -\frac{\sum_{i=1}^{d_\beta-1} b_i}{1 + \lambda_\beta}. \quad (97)$$

So then $h^0(G_4, L) = d_\beta - 1$. However, if we assume that $\lambda_\alpha = 1$ and $\lambda_\beta \neq 1$, then any $a_0 \in \mathbb{C}$ solves the first condition. In addition, we find

$$b_0 = \lambda_\beta b_{d_\beta}, \quad b_{d_\beta} = \frac{a_0 - \sum_{i=1}^{d_\beta-1} b_i}{1 + \lambda_\beta}. \quad (98)$$

So then $h^0(G_4, L) = d_\beta$ and G_4 is jumping for $d_\alpha = 0$ and $d_\beta > 0$.

It remains to study situation with $d_\alpha, d_\beta \geq 1$.

- $d_\alpha = d_\beta = 1$:

Then the gluing conditions are

$$a_0 = \lambda_\alpha a_1, \quad b_0 = \lambda_\beta b_1, \quad a_1 (1 + \lambda_\alpha) = b_1 (1 + \lambda_\beta). \quad (99)$$

If $\lambda_\alpha = \lambda_\beta = -1$, then the third condition is trivial and one has $h^0(G_4, L) = 2$. However, if $(\lambda_\alpha, \lambda_\beta) \neq (-1, -1)$, then $h^0(G_4, L) = 1$. So G_4 is jumping for $d_\alpha = d_\beta = 1$.

- $d_\alpha = 1$ and $d_\beta > 1$:

Then the gluing conditions are

$$a_0 = \lambda_\alpha a_1, \quad b_0 = \lambda_\beta b_{d_\beta}, \quad a_1(1 + \lambda_\alpha) = b_{d_\beta}(1 + \lambda_\beta) + b_1 + \sum_{i=2}^{d_\beta-1} b_i. \quad (100)$$

Hence, $h^0(G_4, L) = d_\alpha + d_\beta - 1$ for all $L \in \mathcal{F}$ and G_4 is non-jumping.

- $d_\alpha, d_\beta > 1$:

Then the gluing conditions are

$$a_0 = \lambda_\alpha a_{d_\alpha}, \quad b_0 = \lambda_\beta b_{d_\beta}, \quad a_{d_\alpha}(1 + \lambda_\alpha) + a_1 + \sum_{i=2}^{d_\alpha-1} a_i = b_{d_\beta}(1 + \lambda_\beta) + \sum_{i=1}^{d_\beta-1} b_i. \quad (101)$$

Hence, $h^0(G_4, L) = d_\alpha + d_\beta - 1$ for all $L \in \mathcal{F}$ and G_4 is non-jumping.

This completes the argument. ■

Proposition A.4. G_5 is jumping iff $0 \leq d_\alpha, d_\beta \leq 2$:



Proof

Certainly, for $d_\alpha, d_\beta < 0$, G_5 is non-jumping. Before we proceed, let us fix notation. For $V_1 = \mathbb{P}_\alpha^1$ we use the homogeneous coordinates $[x : y]$ and for $V_2 = \mathbb{P}_\beta^1$ we use the homogeneous coordinates $[u : v]$. Thereby, we can write $\varphi_\alpha \in H^0(V_1, L|_{V_1})$ and $\varphi_\beta \in H^0(V_2, L|_{V_2})$ as follows:

$$\varphi_\alpha = \sum_{i=0}^{d_\alpha} a_i x^i y^{d_\alpha-i}, \quad \varphi_\beta = \sum_{i=0}^{d_\beta} b_i u^i v^{d_\beta-i}. \quad (103)$$

By an $\text{SL}(2, \mathbb{C})$ transformation, we position the first three nodes at $n_1 = [1 : 0]$, $n_2 = [0 : 1]$ and $n_3 = [1 : 1]$ – each with descent data λ_1, λ_0 and λ_2 . The position of the fourth node is not fixed by an $\text{SL}(2, \mathbb{C})$ transformation. We parametrize the position of this fourth node on $V_1 = \mathbb{P}_\alpha^1$ as $[A : 1]$ and on $V_2 = \mathbb{P}_\beta^1$ as $[B : 1]$, where $A, B \in \mathbb{C} \setminus \{0, 1\}$.

Let us begin by looking at $d_\alpha < 0$ and $d_\beta \geq 0$. Then the gluing conditions are as follows:

$$0 = \lambda_1 \cdot b_{d_\beta}, \quad 0 = \lambda_0 \cdot b_0, \quad 0 = \lambda_2 \cdot \sum_{i=1}^{d_\beta-1} b_i, \quad 0 = \sum_{i=1}^{d_\beta-1} b_i \cdot B^i. \quad (104)$$

So then $h^0(G_5, L) = \max\{0, d_\beta - 3\}$ for all $L \in \mathcal{F}$, i.e. G_5 is non-jumping. It remains to discuss $d_\alpha, d_\beta \geq 0$. We do so by discussing several cases:

- $d_\alpha = d_\beta = 0$:

Then the gluing conditions are as follows:

$$a_0 = \lambda_1 \cdot b_0, \quad a_0 = \lambda_0 \cdot b_0, \quad a_0 = \lambda_2 \cdot b_2, \quad a_0 = b_0. \quad (105)$$

So $h^0(G_5, L) = 1$ iff $\lambda_0 = \lambda_1 = \lambda_2 = 1$ and otherwise $h^0(G_5, L) = 0$. Hence, G_5 is jumping for $d_\alpha = d_\beta = 0$.

- $d_\alpha = 0$ and $d_\beta = 1$:

Then the gluing conditions are as follows:

$$a_0 = \lambda_1 \cdot b_1, \quad a_0 = \lambda_0 \cdot b_0, \quad a_0 = \lambda_2 \cdot (b_0 + b_1), \quad a_0 = b_0 + b_1 \cdot B. \quad (106)$$

Equivalently, we have

$$b_1 = \frac{a_0}{\lambda_1}, \quad b_0 = \frac{a_0}{\lambda_0}, \quad 0 = a_0 \cdot \left(\frac{\lambda_2}{\lambda_0} + \frac{\lambda_2}{\lambda_1} - 1 \right), \quad 0 = a_0 \cdot \left(\frac{1}{\lambda_0} + \frac{B}{\lambda_1} - 1 \right). \quad (107)$$

Take $B = 2$, $\lambda_0 = 2$, $\lambda_1 = 4$ and $\lambda_2 = \frac{4}{3}$. Then the last two conditions are trivial and $h^0(G_5, L) = 1$. However, for generic B , λ_0 , λ_1 and λ_2 , we have $h^0(G_5, L) = 0$. So G_5 is jumping for $d_\alpha = 0$ and $d_\beta = 1$.

- $d_\alpha = d_\beta = 1$:

Then the gluing conditions are as follows:

$$a_1 = \lambda_1 \cdot b_1, \quad a_0 = \lambda_0 \cdot b_0, \quad a_0 + a_1 = \lambda_2 \cdot (b_0 + b_1), \quad a_0 + a_1 A = b_0 + b_1 B. \quad (108)$$

Equivalently, we have

$$b_1 = \frac{a_1}{\lambda_1}, \quad b_0 = \frac{a_0}{\lambda_0}, \quad 0 = a_0 \cdot \left(\frac{\lambda_2}{\lambda_0} - 1 \right) + a_1 \cdot \left(\frac{\lambda_2}{\lambda_1} - 1 \right), \quad (109)$$

$$0 = a_0 \cdot \left(\frac{1}{\lambda_0} - 1 \right) + a_1 \cdot \left(\frac{B}{\lambda_1} - A \right). \quad (110)$$

Take $\lambda_0 = \lambda_1 = \lambda_2 = 1$ and $A = B = 2$. Then the last two conditions are trivial and $h^0(G_5, L) = 2$. But for generic λ_0 , λ_1 , λ_2 , A and B , we have $h^0(G_5, L) < 2$. So G_5 is jumping for $d_\alpha = d_\beta = 1$.

- $d_\alpha = 0$ and $d_\beta = 2$:

Then, the gluing conditions become

$$a_0 = \lambda_1 \cdot b_2, \quad a_0 = \lambda_0 \cdot b_0, \quad b_0 \cdot (\lambda_0 - \lambda_2) + b_2 \cdot (\lambda_1 - \lambda_2) = \lambda_2 \cdot b_1, \quad (111)$$

$$b_0 (\lambda_0 - 1) + b_2 (\lambda_1 - B^2) = B \cdot b_1. \quad (112)$$

Equivalently, we can write

$$b_0 = \frac{a_0}{\lambda_0}, \quad b_2 = \frac{a_0}{\lambda_1}, \quad b_1 = a_0 \cdot \left(\frac{2}{\lambda_2} - \frac{1}{\lambda_0} - \frac{1}{\lambda_1} \right), \quad (113)$$

$$0 = a_0 \cdot \left(\frac{2B}{\lambda_2} + \frac{1-B}{\lambda_0} + \frac{B(B-1)}{\lambda_1} - 2 \right). \quad (114)$$

Take $B = \lambda_2 = 1$. Then these conditions are satisfied for all $\alpha_0 \in \mathbb{C}$ and so $h^0(G_5, L) = 1$. However, for generic λ_0 , λ_1 , λ_2 and B , the last condition will only be satisfied when $\alpha_0 = 0$ and so, $h^0(G_5, L) = 0$. Consequently, G_5 is jumping for $d_\alpha = 0$ and $d_\beta = 2$.

- $d_\alpha = 1$ and $d_\beta = 2$:

Then, the gluing conditions are

$$a_1 = \lambda_1 \cdot b_2, \quad a_0 = \lambda_0 \cdot b_0, \quad b_0 \cdot (\lambda_0 - \lambda_2) + b_2 \cdot (\lambda_1 - \lambda_2) = \lambda_2 \cdot b_1, \quad (115)$$

$$b_0 (\lambda_0 - 1) + b_2 (\lambda_1 A - B^2) = B \cdot b_1. \quad (116)$$

Equivalently, we have

$$a_1 = \lambda_1 \cdot b_2, \quad a_0 = \lambda_0 \cdot b_0, \quad (117)$$

$$b_1 = \frac{b_0 \cdot (\lambda_0 - \lambda_2) + b_2 \cdot (\lambda_1 - \lambda_2)}{\lambda_2}, \quad (118)$$

$$0 = b_0 [\lambda_2 (\lambda_0 - 1) + B (\lambda_2 - \lambda_0)] + b_2 [A \lambda_1 \lambda_2 + B (\lambda_2 - \lambda_1) - B^2 \lambda_2]. \quad (119)$$

Take $\lambda_0 = \lambda_1 = \lambda_2 = 1$, $A = 4$ and $B = 2$. Then the last condition is trivially satisfied for all $b_0, b_2 \in \mathbb{C}$. And so $h^0(G_5, L) = 2$. However, for generic $\lambda_0, \lambda_1, \lambda_2, A$ and B we find $h^0(G_5, L) = 1$ and so G_5 is jumping for $d_\alpha = 1$ and $d_\beta = 2$.

- $d_\alpha = d_\beta = 2$:

Then, the gluing conditions are

$$a_2 = \lambda_1 \cdot b_2, \quad a_0 = \lambda_0 \cdot b_0, \quad b_0 \cdot (\lambda_0 - \lambda_2) + b_2 \cdot (\lambda_1 - \lambda_2) = \lambda_2 \cdot b_1 - a_1, \quad (120)$$

$$b_0 (\lambda_0 - 1) + b_2 (\lambda_1 A^2 - B^2) = b_1 B - a_1 A. \quad (121)$$

Equivalently, we can write

$$a_2 = \lambda_1 \cdot b_2, \quad a_0 = \lambda_0 \cdot b_0, \quad (122)$$

$$a_1 = \lambda_2 \cdot b_1 - b_0 \cdot (\lambda_0 - \lambda_2) - b_2 \cdot (\lambda_1 - \lambda_2), \quad (123)$$

$$0 = b_0 \cdot [A (\lambda_2 - \lambda_0) + \lambda_0 - 1] + b_1 \cdot [A \lambda_2 - B] + b_2 \cdot [\lambda_1 A^2 - B^2 + A (\lambda_2 - \lambda_1)]. \quad (124)$$

Take $\lambda_0 = \lambda_1 = \lambda_2 = 1$ and $A = B = 2$. Then the last condition is trivial and we have $h^0(G_5, L) = 3$. However, for generic $\lambda_0, \lambda_1, \lambda_2, A$ and B , the last condition is non-trivial and we have $h^0(G_5, L) = 2$. Hence, G_5 is jumping for $d_\alpha = d_\beta = 2$.

- $d_\alpha, d_\beta > 2$:

Then the four conditions become

$$a_{d_\alpha} = \lambda_1 \cdot b_{d_\beta}, \quad (125)$$

$$a_0 = \lambda_0 b_0, \quad (126)$$

$$a_1 = -b_0 \cdot (\lambda_0 - \lambda_2) - b_{d_\beta} \cdot (\lambda_1 - \lambda_2) - \sum_{i=2}^{d_\alpha-1} a_i + \lambda_2 \cdot \sum_{i=1}^{d_\beta-1} b_i, \quad (127)$$

$$= - \sum_{i=2}^{d_\alpha-1} a_i + \Gamma(\mathbf{b}, \lambda_0, \lambda_1, \lambda_2), \quad (128)$$

$$a_1 A + \sum_{i=2}^{d_\alpha-1} a_i A^i = \sum_{i=1}^{d_\beta-1} b_i B^i - b_0 (\lambda_0 - 1) + b_{d_\beta} (\lambda_1 A^{d_\alpha} - B^{d_\beta}). \quad (129)$$

By plugging the third into the fourth condition we find

$$\sum_{i=2}^{d_\alpha-1} a_i (A^i - A) = \sum_{i=1}^{d_\beta-1} b_i B^i - b_0 (\lambda_0 - 1) + b_{d_\beta} (\lambda_1 A^{d_\alpha} - B^{d_\beta}) - A \cdot \Gamma(\mathbf{b}, \lambda_0, \lambda_1, \lambda_2), \quad (130)$$

$$= \Gamma_2(A, B, \mathbf{b}, \lambda_0, \lambda_1, \lambda_2) \quad (131)$$

Since $A \in \mathbb{C} \setminus \{0, 1\}$, this is equivalent to

$$a_2 = \frac{\Gamma_2(A, B, \mathbf{b}, \lambda_0, \lambda_1, \lambda_2) - \sum_{i=3}^{d_\alpha-1} a_i (A^i - A)}{A^2 - A}. \quad (132)$$

Hence, G_5 is non-jumping for $2 < d_\alpha, d_\beta$.

This completes the argument. ■

A.2. Elliptic circuits

Proposition A.5. G_6 is jumping for $d = 0$:

$$\textcircled{d=0} \quad (133)$$

Proof

This is well-known for line bundles on elliptic curves. ■

Proposition A.6. The following configuration G_7 is jumping for $d \geq 1$:

$$\textcircled{d} \quad (134)$$

Proof

Let us denote the nodes as $p, q \in E$. Assume that $L|_E = \mathcal{O}_E((d+2) \cdot r - p - q)$ with $r \in E - \{p, q\}$. Then it holds

$$H^0(E, L|_E) = \{f: E \rightarrow \overline{\mathbb{C}} \text{ rational}, \text{div}(f) \geq -(d+2) \cdot r + p + q\}. \quad (135)$$

Consequently, any $\varphi \in H^0(E, L|_E)$ vanishes at the points p and q . Therefore, the gluing condition is trivially satisfied and we find $h^0(G_7, L) = d > d - 1$. ■

Proposition A.7. G_8 is jumping for $d \geq 1$:

$$\textcircled{d} \text{---} \textcircled{1} \quad (136)$$

Proof

Choose homogeneous coordinates $[x: y]$ for the \mathbb{P}^1 , descent data $\lambda = 1$ for the self-edge of this rational curve and fix the position of the end points of the node encoded by this self edge to $[1: 0]$ and $[0: 1]$ by an $SL(2, \mathbb{C})$ transformation. The most general section on this \mathbb{P}^1 , which satisfies the gluing condition via the self-edge is

$$\varphi([x: y]) = \alpha \lambda x + \alpha y, \quad \alpha \in \mathbb{C} \text{ arbitrary but fixed.} \quad (137)$$

Next, take the node connecting the \mathbb{P}^1 to the elliptic curve E to be $[1: 1]$ and the section on E to be ψ . Then the final condition to be imposed is

$$\psi(p) = \alpha \cdot (\lambda + 1). \quad (138)$$

Let us assume that $\lambda = -1$ and that

$$L|_E = \mathcal{O}_E((d+1) \cdot r - p), \quad r \in E - \{p\}. \quad (139)$$

Then $\psi(p) = 0$ and the condition $\psi(p) = \alpha \cdot (\lambda + 1)$ is satisfied for all $\alpha \in \mathbb{C}$. Consequently, we then find $h^0(G_8, L) = d + 1 > (d + 2) - 2$. Hence, G_8 is jumping for $d \geq 1$. ■

Proposition A.8. G_9 is jumping for $d \geq 1$:



Proof

We take coordinates $[x : y]$ for the \mathbb{P}^1 and place the nodes on this curve at $[1 : 0]$, $[0 : 1]$ and $[1 : 1]$. We label the corresponding points on E as p_1 , p_2 and p_3 . Hence, the gluing conditions to be imposed are

$$\psi(p_1) = \lambda_1 \alpha, \quad (141)$$

$$\psi(p_2) = \lambda_2 \beta, \quad (142)$$

$$\psi(p_3) = \alpha + \beta. \quad (143)$$

Since $\lambda_1, \lambda_2 \in \mathbb{C}^*$, we always have

$$\frac{\psi(p_1)}{\lambda_1} = \alpha, \quad \frac{\psi(p_2)}{\lambda_2} = \beta. \quad (144)$$

This uniquely determines the section on the \mathbb{P}^1 . It remains to satisfy the third condition with the sections on E :

$$\psi(p_3) = \frac{\psi(p_1)}{\lambda_1} + \frac{\psi(p_2)}{\lambda_2}. \quad (145)$$

Let us assume that

$$L|_E = \mathcal{O}_E((d_\alpha + 3) \cdot r - p_1 - p_2 - p_3), \quad r \in E - \{p_1, p_2, p_3\}. \quad (146)$$

Then for every $\psi \in H^0(E, L|_E)$ it holds $\psi(p_1) = \psi(p_2) = \psi(p_3) = 0$. Consequently, the condition in eq. (145) is trivially satisfied and we $h^0(G_9, L) = d > (d + 2) - 3$. \blacksquare

Proposition A.9. G_{10} is jumping for $d \geq 1$:



Proof

We pick coordinates $[x : y]$ and $[u : v]$ for the two \mathbb{P}^1 s and fix the node positions to $[1 : 0]$ and $[0 : 1]$ respectively. Take the descent data to be λ_1 and λ_2 along these two nodes. The most general section on the left bottom \mathbb{P}^1 be

$$\varphi_a = \alpha_1 x + \alpha_2 y. \quad (148)$$

Then the sections on the bottom right \mathbb{P}^1 are uniquely fixed to be

$$\varphi_b = \lambda_1 \alpha_1 u + \lambda_2 \alpha_2 v. \quad (149)$$

The nodes of the \mathbb{P}^1 towards the elliptic curve can be taken to be $[1 : 1]$. We denote the corresponding points on E as p and q . Let the most general section on E be ψ . Then we impose the following conditions:

$$\psi(p) = \alpha_1 + \alpha_2, \quad \psi(q) = \lambda_1 \alpha_1 + \lambda_2 \alpha_2. \quad (150)$$

Equivalently, we have

$$\alpha_2 = \psi(p) - \alpha_1, \quad \psi(q) - \lambda_2 \psi(p) = (\lambda_1 - \lambda_2) \alpha_1. \quad (151)$$

Let us focus on $\lambda_1 = \lambda_2$ and

$$L|_E = \mathcal{O}_E((d+2) \cdot r - p - q), \quad r \in E - \{p, q\}. \quad (152)$$

Then the condition $\psi(q) - \lambda_2 \psi(p) = (\lambda_1 - \lambda_2) \alpha_1$ is trivially satisfied and we find $h^0(G_{10}, L) = d+1 > (d+2+2) - 4$. This shows that G_{10} is jumping for $d \geq 1$. ■

References

- [1] C. Vafa, *Evidence for F-theory*, *Nuclear Physics B* **469** (Jun, 1996) 403–415, [hep-th/9602022]. 3
- [2] D. R. Morrison and C. Vafa, *Compactifications of F-theory on Calabi-Yau threefolds. (I)*, *Nuclear Physics B* **473** (Aug, 1996) 74–92, [hep-th/9602114]. 3
- [3] D. R. Morrison and C. Vafa, *Compactifications of F-theory on Calabi-Yau threefolds (II)*, *Nuclear Physics B* **476** (Sep, 1996) 437–469, [hep-th/9603161]. 3
- [4] M. Cvetič, J. Halverson, L. Lin, M. Liu and J. Tian, *Quadrillion F-Theory Compactifications with the Exact Chiral Spectrum of the Standard Model*, *Phys. Rev. Lett.* **123** (2019) 101601, [1903.00009]. 3, 4, 5, 7, 29
- [5] M. Bies, M. Cvetič, R. Donagi, M. Liu and M. Ong, *Root bundles and towards exact matter spectra of F-theory MSSMs*, *Journal of High Energy Physics* **09** (2021) 076, [2102.10115]. 3, 4, 5, 6, 7, 8, 29, 31
- [6] M. Bies, M. Cvetič and M. Liu, *Statistics of limit root bundles relevant for exact matter spectra of F-theory MSSMs*, *Phys. Rev. D* **104** (2021) L061903, [2104.08297]. 3, 4, 5, 6, 7, 8, 23, 29, 31
- [7] M. Bies, M. Cvetič, R. Donagi and M. Ong, *Brill-Noether-general limit root bundles: absence of vector-like exotics in F-theory Standard Models*, *Journal of High Energy Physics* **11** (2022) 4, [2205.00008]. 3, 4, 5, 6, 7, 8, 23, 24, 25, 26, 27, 29, 30
- [8] M. Cvetič, J. Halverson, G. Shiu and W. Taylor, *Snowmass White Paper: String Theory and Particle Physics*, 2204.01742. 3
- [9] T. Weigand, *F-theory*, *PoS TASI2017* (2018) 016, [1806.01854]. 3
- [10] P. Candelas, G. T. Horowitz, A. Strominger and E. Witten, *Vacuum configurations for superstrings*, *Nuclear Physics B* **258** (1985) 46–74. 3
- [11] B. R. Greene, K. H. Kirklin, P. J. Miron and G. G. Ross, *A superstring-inspired standard model*, *Physics Letters B* **180** (1986) 69–76. 3
- [12] V. Braun, Y.-H. He, B. A. Ovrut and T. Pantev, *A heterotic standard model*, *Physics Letters B* **618** (Jul, 2005) 252–258, [hep-th/0501070]. 3

- [13] V. Bouchard and R. Donagi, *An $SU(5)$ heterotic standard model*, *Physics Letters B* **633** (Feb, 2006) 783–791, [[hep-th/0512149](#)]. 3
- [14] V. Bouchard, M. Cvetič and R. Donagi, *Tri-linear couplings in an heterotic minimal supersymmetric Standard Model*, *Nuclear Physics B* **745** (Jun, 2006) 62–83, [[hep-th/0602096](#)]. 3
- [15] L. B. Anderson, J. Gray, Y.-H. He and A. Lukas, *Exploring Positive Monad Bundles And A New Heterotic Standard Model*, *Journal of High Energy Physics* **02** (2010) 054, [[0911.1569](#)]. 3
- [16] L. B. Anderson, J. Gray, A. Lukas and E. Palti, *Two Hundred Heterotic Standard Models on Smooth Calabi-Yau Threefolds*, *Phys. Rev.* **D84** (2011) 106005, [[1106.4804](#)]. 3
- [17] L. B. Anderson, J. Gray, A. Lukas and E. Palti, *Heterotic line bundle standard models*, *Journal of High Energy Physics* **2012** (Jun, 2012) , [[1202.1757](#)]. 3
- [18] M. Berkooz, M. R. Douglas and R. G. Leigh, *Branes intersecting at angles*, *Nuclear Physics B* **480** (Nov, 1996) 265–278, [[hep-th/9606139](#)]. 3
- [19] G. Aldazabal, S. Franco, L. E. Ibáñez, R. Rabadan and A. M. Uranga, *$D=4$ chiral string compactifications from intersecting branes*, *Journal of Mathematical Physics* **42** (Jul, 2001) 3103–3126, [[hep-th/0011073](#)]. 3
- [20] G. Aldazabal, S. Franco, L. E. Ibáñez, R. Rabadan and A. M. Uranga, *Intersecting brane worlds*, *Journal of High Energy Physics* **02** (2001) 047, [[hep-ph/0011132](#)]. 3
- [21] L. E. Ibáñez, F. Marchesano and R. Rabadan, *Getting just the standard model at intersecting branes*, *Journal of High Energy Physics* **2001** (Nov, 2001) 002–002, [[hep-th/0105155](#)]. 3
- [22] R. Blumenhagen, B. Kors, D. Lüst and T. Ott, *The Standard Model from stable intersecting brane world orbifolds*, *Nuclear Physics B* **616** (Nov, 2001) 3–33, [[hep-th/0107138](#)]. 3
- [23] M. Cvetič, G. Shiu and A. M. Uranga, *Chiral four-dimensional $N=1$ supersymmetric type IIA orientifolds from intersecting $D6$ -branes*, *Nuclear Physics B* **615** (Nov, 2001) 3–32, [[hep-th/0107166](#)]. 3
- [24] M. Cvetič, G. Shiu and A. M. Uranga, *Three family supersymmetric standard - like models from intersecting brane worlds*, *Phys. Rev. Lett.* **87** (2001) 201801, [[hep-th/0107143](#)]. 3
- [25] R. Blumenhagen, M. Cvetič, P. Langacker and G. Shiu, *Toward realistic intersecting D -brane models*, *Annual Review of Nuclear and Particle Science* **55** (Dec, 2005) 71–139, [[hep-th/0502005](#)]. 3
- [26] T. L. Gómez, S. Lukic and I. Sols, *Constraining the Kähler Moduli in the Heterotic Standard Model*, *Communications in Mathematical Physics* **276** (Sep, 2007) 1–21, [[hep-th/0512205](#)]. 3
- [27] V. Bouchard and R. Donagi, *On heterotic model constraints*, *Journal of High Energy Physics* **2008** (Aug, 2008) 060–060, [[0804.2096](#)]. 3

- [28] J. J. Heckman, *Particle Physics Implications of F-theory*, *Ann. Rev. Nucl. Part. Sci.* **60** (2010) 237–265, [1001.0577]. 3
- [29] R. Donagi and M. Wijnholt, *Model Building with F-Theory*, *Adv. Theor. Math. Phys.* **15** (2011) 1237–1317, [0802.2969]. 3
- [30] J. Marsano and S. Schafer-Nameki, *Yukawas, G-flux, and Spectral Covers from Resolved Calabi-Yau's*, *Journal of High Energy Physics* **11** (2011) 098, [1108.1794]. 3
- [31] A. P. Braun, A. Collinucci and R. Valandro, *G-flux in F-theory and algebraic cycles*, *Nucl. Phys. B* **856** (2012) 129–179, [1107.5337]. 3
- [32] T. W. Grimm and H. Hayashi, *F-theory fluxes, Chirality and Chern-Simons theories*, *Journal of High Energy Physics* **03** (2012) 027, [1111.1232]. 3
- [33] S. Krause, C. Mayrhofer and T. Weigand, *Gauge Fluxes in F-theory and Type IIB Orientifolds*, *Journal of High Energy Physics* **08** (Aug, 2012) 119, [1202.3138]. 3
- [34] S. Krause, C. Mayrhofer and T. Weigand, *G_4 -flux, chiral matter and singularity resolution in F-theory compactifications*, *Nuclear Physics B* **858** (May, 2012) 1–47, [1109.3454]. 3, 31
- [35] K. Intriligator, H. Jockers, P. Mayr, D. R. Morrison and M. R. Plesser, *Conifold Transitions in M-theory on Calabi-Yau Fourfolds with Background Fluxes*, *Adv. Theor. Math. Phys.* **17** (2013) 601–699, [1203.666]. 3
- [36] R. Donagi and M. Wijnholt, *Higgs Bundles and UV Completion in F-Theory*, *Commun. Math. Phys.* **326** (2014) 287–327, [0904.1218]. 3
- [37] V. Braun, T. W. Grimm and J. Keitel, *Geometric Engineering in Toric F-Theory and GUTs with $U(1)$ Gauge Factors*, *Journal of High Energy Physics* **12** (2013) 069, [1306.0577]. 3
- [38] M. Cvetič, A. Grassi, D. Klevers and H. Piragua, *Chiral four-dimensional F-theory compactifications with $SU(5)$ and multiple $U(1)$ -factors*, *Journal of High Energy Physics* **04** (2014) 010, [1306.3987]. 3
- [39] M. Cvetič, D. Klevers, D. K. M. Peña, P.-K. Oehlmann and J. Reuter, *Three-Family Particle Physics Models from Global F-theory Compactifications*, *Journal of High Energy Physics* **08** (2015) 087, [1503.02068]. 3, 31
- [40] L. Lin, C. Mayrhofer, O. Till and T. Weigand, *Fluxes in F-theory Compactifications on Genus-One Fibrations*, *Journal of High Energy Physics* **01** (2016) 098, [1508.00162]. 3
- [41] L. Lin and T. Weigand, *G_4 -flux and standard model vacua in F-theory*, *Nuclear Physics B* **913** (Dec, 2016) 209–247, [1604.04292]. 3, 31
- [42] P. Jefferson, W. Taylor and A. P. Turner, *Chiral matter multiplicities and resolution-independent structure in 4D F-theory models*, 2108.07810. 3
- [43] P. Jefferson and A. P. Turner, *Generating functions for intersection products of divisors in resolved F-theory models*, *Nucl. Phys. B* **991** (2023) 116177, [2206.11527]. 3

- [44] M. Cvetič, L. Lin, M. Liu and P.-K. Oehlmann, *An F-theory Realization of the Chiral MSSM with \mathbb{Z}_2 -Parity*, *Journal of High Energy Physics* **09** (2018) 089, [1807.01320]. 3, 31
- [45] P. Jefferson, W. Taylor and A. P. Turner, *Chiral spectrum of the universal tuned $(SU(3) \times SU(2) \times U(1))/\mathbb{Z}_6$ 4D F-theory model*, *Journal of High Energy Physics* **02** (2023) 254, [2210.09473]. 3, 31
- [46] M. Bies, C. Mayrhofer, C. Pehle and T. Weigand, *Chow groups, Deligne cohomology and massless matter in F-theory*, 1402.5144. 4, 7
- [47] M. Bies, C. Mayrhofer and T. Weigand, *Gauge Backgrounds and Zero-Mode Counting in F-Theory*, *Journal of High Energy Physics* **11** (2017) 081, [1706.04616]. 4, 7
- [48] M. Bies, *Cohomologies of coherent sheaves and massless spectra in F-theory*. PhD thesis, Heidelberg U., 2, 2018. 1802.08860. 10.11588/heidok.00024045. 4, 7
- [49] M. F. Atiyah, *Riemann surfaces and spin structures*, *Annales Scientifiques de L'Ecole Normale Supérieure* **4** (1971) 47–62. 4, 8
- [50] D. Mumford, *Theta characteristics of an algebraic curve*, *Ann. Sci. Ecole Norm. Sup* **4** (1971) 181–192. 4, 8
- [51] D. R. Grayson and M. E. Stillman, “Macaulay2, a software system for research in algebraic geometry.” Available at <http://www.math.uiuc.edu/Macaulay2/>, 2023. 4
- [52] The Sage Developers, “SageMath, the Sage Mathematics Software System (Version 9.8).” <https://www.sagemath.org>, 2023. 4
- [53] The OSCAR Team, “OSCAR – Open Source Computer Algebra Research system, Version 0.12.0-DEV.” <https://www.oscar-system.org>, 2023. 4
- [54] Decker, Wolfram and Eder, Christian and Fieker, Claus and Horn, Max and Joswig, Michael, ed., *The OSCAR book*. 2024. 4
- [55] J. Carifio, J. Halverson, D. Krioukov and B. D. Nelson, *Machine Learning in the String Landscape*, *Journal of High Energy Physics* **09** (2017) 157. 4
- [56] J. Halverson, B. Nelson and F. Ruehle, *Branes with Brains: Exploring String Vacua with Deep Reinforcement Learning*, *Journal of High Energy Physics* **06** (2019) 003, [1903.11616]. 4
- [57] S. Abel, A. Constantin, T. R. Harvey and A. Lukas, *String Model Building, Reinforcement Learning and Genetic Algorithms*, in *Nankai Symposium on Mathematical Dialogues: In celebration of S.S.Chern's 110th anniversary*, 11, 2021. 2111.07333. 4
- [58] M. Larfors, A. Lukas, F. Ruehle and R. Schneider, *Learning Size and Shape of Calabi-Yau Spaces*, *arXiv* (11, 2021) , [2111.01436]. 4
- [59] S. Abel, A. Constantin, T. R. Harvey, A. Lukas and L. A. Nutricati, *Decoding Nature with Nature's Tools: Heterotic Line Bundle Models of Particle Physics with Genetic Algorithms and Quantum Annealing*, 2306.03147. 4
- [60] F. Ruehle, *Data science applications to string theory*, *Phys. Rept.* **839** (2020) 1–117. 4

- [61] M. Bies, M. Cvetič, R. Donagi, L. Lin, M. Liu and F. Ruehle, *Machine Learning and Algebraic Approaches towards Complete Matter Spectra in 4d F-theory*, *Journal of High Energy Physics* **01** (2021) 196, [2007.00009]. 4
- [62] M. Bies, M. Cvetič, R. Donagi, L. Lin, M. Liu and F. Ruehle, “Database.” <https://github.com/Learning-line-bundle-cohomology>, 2020. 4
- [63] The Toric Varieties project authors, “The ToricVarieties project.” https://github.com/homalg-project/ToricVarieties_project, 2019–2023. 4
- [64] A. Brill and M. Noether, *Ueber die algebraischen Functionen und ihre Anwendung in der Geometrie*, *Mathematische Annalen* **7** (1874) 269–310. 4
- [65] D. Eisenbud, M. Green and J. Harris, *Cayley-Bacharach theorems and conjectures*, *Bulletin of the American Mathematical Society* **33** (Jul, 1996) 295–325. 4
- [66] T. Watari, *Vector-like pairs and Brill–Noether theory*, *Physics Letters B* **762** (Nov, 2016) 145–150, [1608.00248]. 4
- [67] M. Bies, *Root bundles: Applications to F-theory Standard Models*, 3, 2023. 2303.08144. 4, 7, 8
- [68] M. Liu, *F-Theory Realizations Of Exact MSSM Matter Spectra*. PhD thesis, UPenn, Philadelphia, 2022. <https://repository.upenn.edu/edissertations/4544>. 4
- [69] L. Caporaso, C. Casagrande and M. Cornalba, *Moduli of Roots of Line Bundles on Curves*, *Transactions of the American Mathematical Society* **359** (2007) 3733–3768, [math/0404078]. 5, 8, 29, 31
- [70] M. Kreuzer and H. Skarke, *Classification of reflexive polyhedra in three-dimensions*, *Adv. Theor. Math. Phys.* **2** (1998) 853–871, [hep-th/9805190]. 5, 8, 29, 30
- [71] J. Halverson and J. Tian, *Cost of seven-brane gauge symmetry in a quadrillion F-theory compactifications*, *Phys. Rev. D* **95** (2017) 026005, [1610.08864]. 5, 9, 28, 29, 30
- [72] V. V. Batyrev, *Dual polyhedra and mirror symmetry for Calabi-Yau hypersurfaces in toric varieties*, *J. Alg. Geom.* **3** (1994) 493–545, [alg-geom/9310003]. 5, 8
- [73] E. Perevalov and H. Skarke, *Enhanced gauged symmetry in type II and F theory compactifications: Dynkin diagrams from polyhedra*, *Nuclear Physics B* **505** (Nov, 1997) 679–700, [hep-th/9704129]. 5
- [74] D. A. Cox and S. Katz, *Mirror Symmetry and Algebraic Geometry*. Mathematical surveys and monographs. American Mathematical Society, 1999, <https://www.ams.org/books/surv/068/>. 5
- [75] F. Rohsiepe, *Lattice polarized toric K3 surfaces*, hep-th/0409290. 5
- [76] A. P. Braun, C. Long, L. McAllister, M. Stillman and B. Sung, *The Hodge Numbers of Divisors of Calabi-Yau Threefold Hypersurfaces*, *Fortschritte der Physik* **68** (2020) 2000087, [1712.04946]. 5
- [77] M. Bies, “Root counter.” <https://github.com/Julia-meets-String-Theory/RootCounter>, 2023. 6, 25

- [78] J. Harris and I. Morrison, *Moduli of Curves*. Graduate Texts in Mathematics. Springer New York, 1998, <https://doi.org/10.1007/b98867>. 10
- [79] Wolfram Research, Inc., “Mathematica, Version 13.2, Champaign, IL, 2022.” <https://www.wolfram.com/mathematica>. 29
- [80] W. Karush, *Minima of functions of several variables with inequalities as side conditions*. PhD thesis, Thesis (S.M.)—University of Chicago, Department of Mathematics, December, 1939. https://doi.org/10.1007/978-3-0348-0439-4_10. 29
- [81] H. W. Kuhn and A. W. Tucker, *Nonlinear Programming*, pp. 481–492. University of California Press, Berkeley-Los Angeles, California, 1951. https://doi.org/10.1007/978-3-0348-0439-4_11. 29
- [82] M. Cvetič, J. Halverson, L. Lin and C. Long, *Constraints on Standard Model Constructions in F-theory*, *Phys. Rev. D* **102** (2020) 026012, [2004.00630]. 31
- [83] E. Witten, *On flux quantization in M theory and the effective action*, *J. Geom. Phys.* **22** (1997) 1–13, [hep-th/9609122]. 31
- [84] D. S. Freed and E. Witten, *Anomalies in string theory with D-branes*, *Asian J. Math.* **3** (1999) 819, [hep-th/9907189]. 31
- [85] C. Beasley, J. J. Heckman and C. Vafa, *GUTs and Exceptional Branes in F-theory - I*, *Journal of High Energy Physics* **01** (2009) 058, [0802.3391]. 31
- [86] D. S. Eisenbud and J. Harris, *Limit linear series: Basic theory.*, *Inventiones mathematicae* **85** (1986) 337–372. 31
- [87] B. Osserman, *Limit linear series for curves not of compact type*, *Journal für die reine und angewandte Mathematik (Crelles Journal)* (2019) 57–88, [1406.6699]. 31